A STUDY OF THE ROTATING-STALL INCEPTION IN HIGH-SPEED COMPRESSORS

by

Michail Tryfonidis

Submitted to the Department of Aeronautics and Astronautics
in partial fulfillment of the requirements for the degree of

Master of Science

at the

MASSACHUSETTS INSTITUTE OF TECHNOLOGY

May 1994

Author_____

Department of Aeronautics and Astronautics
May 1994

Certified by_____

James D. Paduano
Assistant Professor of Aeronautics and Astronautics
Thesis Supervisor

Accepted by_____

Professor Harold Y. Wachman
Chairman, Department Graduate Commitee

TABLE OF CONTENTS

TABLE OF CONTENTS 3

ABSTRACT 4

ACKNOWLEDGMENTS 6

1. INTRODUCTION 8

2. DATA REDUCTION PROCEDURES 13

3. DATA ANALYSIS RESULTS AND DISCUSSION 19

I STALL INCEPTION TRANSIENTS 19

II PRE-STALL POWER SPECTRA 24

III ROTATING WAVE ENERGY AND COMPRESSOR STABILITY 27

IV WAVE ENERGY AS STALL WARNING 31

V WAVE ENERGY STRENGTH WITH RESPECT TO AXIAL LOCATION AND CORRECTED SPEED 34

VI DISCUSSION 34

4. SUMMARY AND CONCLUSIONS 38

Table 1: Pre-Stall and Fully developed Rotating Stall speeds. 41

Figure 2.1: Simulated compressor 1st Fourier harmonic wave amplitude and phase. 43

Figure 2.2: Spatial spectra of the simulations. 44

Figure 3: Time traces of wall static pressure at 100% corrected speed 45

Figure 3.2: Time evolution of the first two SFC's at 100% corrected speed. 51

Figure 3.3: Time evolution of the first two SFC's at 70% corrected speed. 54

Figure 3.4: Power spectra of the first two SFC's at 100% corrected speed. 55

Figure 3.5: Power spectra of the first two SFC's at 70% corrected speed. 58

Figure 3.6: Waterfall of the first SFC for compressor #4 at 70% corrected speed. 59

Figure 3.7: Waterfalls of the first SFC for compressors #4 at various speeds 61

Figure 3.8: Waterfall of the first SFC for compressor #4 at 70%, 80%, 90% and 100% corrected speed 64

Figure 3.9: Waterfall of the first SFC for compressors #2. 66

Figure 3.10: Waterfall of the first SFC for compressors #5. 67

Figure 3.11: Waterfall of the first SFC for compressors #7. 68

Figure 3.12: Waterfall of the first SFC for compressors #8. 71

Figure 3.13: First SFC traveling wave energy for the 4-stage compressor. 74

Figure 3.14: First SFC traveling wave energy for the 4-stage compressor in expanded scale. 75

Figure 3.15: Traveling wave energy as a function of axial location and % of corrected speed. 76

Figure 3.16: Traveling wave energy as a function of axial location and % of corrected speed w/o rotor frequency. 77

A STUDY OF ROTATING STALL INCEPTION IN HIGH-SPEED COMPRESSORS

by

Michail Tryfonidis

Submitted to the Department of Aeronautics and Astronautics
on May 16, 1994 in partial fulfillment of the requirements for the
degree of Master of Science in Aeronautics and Astronautics

Abstract

High speed compressor data from nine different compressors are shown, to demonstrate similarities in their behavior, and to compare the experimental results to stability theory. We review several previous approaches and discuss their limitations. New methods are introduced and discussed.

In all of the compressors studied, rotating stall precedes surge. In the pre-stall region, all nine compressors support small amplitude (less than 1% of fully developed stall) traveling waves. The strength and the structure of these traveling waves are strong functions of the corrected speed. At the lower corrected speeds a 0.5 to 0.7 times-the-shaft-speed wave is discernible for several rotor revolutions prior to stall. At 100% corrected speed, a signal that travels at the shaft speed dominates the data before stall initiates. The final stall speed is about 0.5 of the rotor speed in every case. A new understanding of compressibility effects on the compressor behavior is used to apply the concept of traveling wave energy as a measure of compressor stability. We show that a warning scheme based on this traveling-wave-energy concept can result in warning times of the order of 100 rotor revolution. In addition, the value of the wave energy is shown to be a strong function of both the axial location and the corrected speed.

Thesis Supervisor: James D. Paduano

Title: Assistant Professor of Aeronautics and Astronautics

ACKNOWLEDGMENTS

Upon completion of this thesis I would like to thank my advisor, Professor J.D. Paduano, for his help in every occasion and for showing understanding when the going got tough. Special thanks also to Professor A.H. Epstein for all his support. Thanks also are appropriate for Dr. G.R. Guenette whose guidance was invaluable. Finally, I would like to thank S. Baghdadi, J.E. Garberoglio and D. Hobbs of Pratt & Whitney; W. Copenhaver, D.A. Hoying, B. Frank and D. Rabe of Wright Laboratory USAF; A. Sehra and S. Etter of Textron Lycoming; C. Freeman and A. Wilson of Rolls-Royce plc; and K. Owen of the US Army. D. Park formatted and edited many of the figures. This work was supported by the US Air Force Office of Scientific Research, Major D. Fant, program monitor, Pratt & Whitney and NASA Lewis Research Center.

1. INTRODUCTION

One of the design limitations that determines compressor performance is the *stall* or *surge* margin. As the throttle that controls the air flow through the compressor closes, the system goes into a fluid instability that causes the pressure ratio across the compressor to fall rapidly. The instability manifests itself as either a one or a two-dimensional phenomenon. Stall is a two-dimensional fluid instability that occurs when the mass flow falls below a certain level. Stall appears in the form of stall cells that rotate around the annulus at approximately 50% of the rotor speed. On the other hand, surge is a one-dimensional instability. In both cases large pressure waves cause high amplitude vibratory motion of the system and degradation of its performance. The conventional way to avoiding unexpected instabilities is to leave a margin of safety (stall margin) during compressor design. One avenue to improving compressor performance is to allow the compressor to operate at flow coefficients below the stall margin by either active or passive means. Such a task requires a thorough understanding of the stall inception process.

To facilitate discussion, we will first define some terms that will appear in this thesis. *Fully developed rotating stall* will refer to large amplitude (50-100% mass flow fluctuations) rotating stall, during which amplitude variations of the stall cell are insignificant. *Stall inception* is the transient from axisymmetric, small perturbation flow conditions to rotating stall, and thus includes large disturbances whose amplitudes change with time. *Pre-stall* refers to the time immediately before stall inception, during which compressor operation is steady but may exhibit small-amplitude (of the order of 1%) dynamics. Perturbations associated with these dynamics are small compared both to stall inception and to fully developed stall perturbations. These three regions -- pre-stall, stall inception and fully developed stall -- are difficult to separate precisely; rather, the terminology allows us to communicate our ideas in a more concise manner.

Using both models and experimental data, researchers have attempted to develop an improved description of rotating stall inception (G.J. Hendricks, 1993). Part of the effort was to try to model the connection between small and large amplitude disturbances and between stall and surge. An accurate description of the stall inception process would be useful not only in stall control (both active and passive) but also in compressor design as well as stall warning and avoidance.

The development of a hydrodynamic stability model by Moore and Greitzer (1986) motivates the methods for studying stall inception in this thesis. McDougal (1989) first introduced the idea of using a circumference array of sensors at one or more axial locations in an attempt to detect circumferential waves of perturbation in pressure or velocity. Two-dimensional hydrodynamic theory predicts that sinusoidal traveling waves will become underdamped near the stall inception point, and thus spatial sinusoids of small amplitude should be detectable before stall inception occurs. Unfortunately, these waves are of very small amplitude and are often hard to pick out through the noise. One can improve of the signal-to-noise ratio by choosing sensors that are not as sensitive to aerodynamic and structural vibrations. This improvement will potentially allow the detection of the small-amplitude waves that would have otherwise been lost in the compressor noisy environment.

The Moore-Greitzer theory predicts *long length scale*, wavelike disturbances, as opposed to the argument developed by Emmons (19) originally and by Day and Freeman (1993) later, which conjectures that *short length scale* disturbances lead to stall. The name "long length scale disturbances" refers to the wavelengths that are comparable to the circumference of the annulus. On the other hand, the short length scale disturbances have lengths comparable to the blade pitch. Day (1993) observed that the engine that he was testing went into stall without first showing any indication of the long length scale perturbations. Instead, he observed only short length scale disturbances a few rotor

revolutions before stall (in the stall-inception region). However, we have been unable to consistently see such perturbations in several of the compressors that we studied.

On the other hand, the long-length-disturbance approach to stall detection has raised two serious questions. First, whether and under what conditions do spatial waves exist in high-speed axial compressors prior to stall inception. Second, if waves do exist, what are the best methods to detect them and to employ their detection in a stall warning scheme.

Several researchers in the past addressed the question of whether waves exist in high-speed compressors. Garnier (1991) investigated a three-stage high-speed compressor. The compressor was a Pratt and Whitney design. When Garnier calculated the spatial Fourier coefficients (SFCs), the magnitude of the second SFC was growing the strongest into stall. The phase speed of the second SFC is more readily discerned than the phase speed of the first SFC. This fact by itself disagrees with the hydrodynamic theory, which predicts that the first SFC is the first Fourier coefficient to grow into stall. Garnier's data gave a very coherent warning of about 100 rotor revs. Comparison of the phase speed of the second SFC as measured at the leading edge of each of the three stator rows showed the signal to be the clearest at the first stage.

Hönen and Gallus (1993) came up with a warning scheme for rotating stall. Specifically, they noticed that the peak level at the characteristic frequency of a stage is an indicator of the aerodynamic load. They also noticed that up to the point of the collapse of the periodic fluctuations, the peak amplitude grows out of the normal noise level, which also rises with increasing aerodynamic load. Finally, they defined a stage load parameter (SL) as a linear function of the power at the peak frequencies of each stage. The behavior of the aerodynamic load is very similar to what we will observe happening to the spatial Fourier harmonics of our systems as they approach instability.

Using Garnier's findings and the concept of long wave disturbances as developed by Moore and Greitzer, other researchers have worked on the improvement of the stall

margin. Paduano (1993) has shown the existence of traveling-wave precursors in a low speed machine as the compressor slowly approached stall. Actively damping the traveling-wave precursors using Inlet Guide Vanes (IGV's) resulted in lowering the flow coefficient at which the compressor grew into fully developed stall.

The high-speed compressor data presented here comes through the cooperation of several industrial and US government organizations. The compressors studied cover over 30 years of design practice, ranging from older concepts to the most advanced approaches. Some are of fixed geometry, some have interstage bleeds, and some have variable IGV's and stators. In all cases, data are time resolved wall static pressure measurements, roughly equally spaced around the annulus, at one or more axial stations. In the cases where there were sensors at more than one stage, the stage that gave the best results appears in the thesis. The compressor designations follow:

Compressor No.	Description
#1	•1-stage civil fan, nacelle in wind tunnel
#2	•1-stage high through flow military fan (Boyer, 1993)
#3	•3-stage core compressor (Garnier, 1991)
#4	•4-stage core compressor (Hoying, 1993)
#5	•5-stage core compressor
#6	•6-stage
#7	•7-stage axial, 1-centrifugal, T-55 data (Owen, 1993)
#8	•8-stage, Viper engine data (Day and Freeman, 1993c)
#9	•2-stage

All compressors used 8 transducers per stage about the circumference except #7 which had 4 and #9 which had 5. The compressors for which the geometry and the steady state performance were available provided a good opportunity to compare the data with the

theory. For the compressors with literature references please note that the data analyzed here might not be the same as those that appeared in previous publications

In the following sections will present: Data reduction procedures, in Chapter 2; Stall-precedes-surge results, in Chapter 3 I; Phase of the spatial Fourier coefficients as evidence of traveling wave existence, in Chapter 3 I; Power spectral density as a measure of the wave energy, in Chapter 3 II; Wave energy and compressor stability, in Chapter 3 III; Integrated wave energy as a warning scheme, in Chapter 3 IV; Wave energy as a function of axial location and corrected speed, in Chapter 3 V; Discussion of the results, in Chapter VI; Summary of the results, in Chapter 4.

2. DATA REDUCTION PROCEDURES

Since the investigation of the existence of modal waves was one of the primary goals of this work, the data reduction procedure is designed to avoid any pre-disposition of the results. Thus, for instance, the data did not pass through any narrow band-pass filters, since this can yield traveling when actually very little wave energy exists.

During the data reduction, the spatial structure of the predicted traveling waves was used to motivate a scheme for detecting traveling of spatially coherent structures. Following the theoretical development of Garnier (1991), we will assume that the pressure perturbations of interest take the following form at a given axial station:

$$\delta P_x(\vartheta, t) = \mathrm{Re}\left\{ \sum_{k=-\infty}^{\infty} a_k(t) \cdot e^{ik\vartheta} \right\} \tag{1}$$

where x indicates the axial station at which the measurements are taken, and $a_k(t)$ are the *spatial* Fourier coefficients of the perturbations (the $a_k(t)$'s will also be called the *harmonics* of the system). According to the linearized hydrodynamic theory of compressor stability, the spatial Fourier coefficients evolve independently and thus constitute the fundamental states of the system. On the other hand, an individual pressure perturbation $\delta P_x(\vartheta_n, t)$ at a given circumferential position ϑ_n, is correlated to that of any other position, and thus it is a combination of dynamic effects which must somehow be distinguished.

One can derive an approximation for $a_k(t)$ from a set of N circumferential measurements of δP_x by using the spatial Fourier transform:

$$a_k(t) = \frac{1}{N} \cdot \sum_{n=1}^{N} \delta P(\vartheta_n, t) \cdot e^{-2\pi i k \vartheta_n} \tag{2}$$

where N must obey the Nyquist criterion for the harmonic k, that is, $N \geq 2k+1$. The sensor locations ϑ_n are usually evenly spaced (as long as sensor spacing is *nearly* even, other frequencies *below* the Nyquist frequency will not alias into the estimate of $a_k(t)$).

The assumption that the spatial Fourier coefficients are independent and that they represent the states of the system diagonalizes the system. Therefore, the states $a_k(t)$ evolve according to independent dynamics. The data reduction procedure described below assumes very little about what these dynamics are, but since one of our goals is to determine whether the dynamics predicted by hydrodynamic stability theory exist, it is important to describe the expected behavior of the system. In the low-speed hydrodynamic model a single eigenvalue dominates the flow through the compressor at each operating point. Therefore, a simple model can be used (see, Garnier):

$$\frac{da_k}{dt} = (\sigma_k - i\omega_k) \cdot a_k + V(t) \tag{3}$$

where *V(t)* represents the random excitation of the system related to the unsteady aerodynamics of the compressor, inflow distortions, etc. The assumption that the excitation is white noise is a reasonable one since the character of this noise is unknown in compressors and engines. Figures 2.1 and 2.2 show a computer generated simulation of a system that obeys equation (3).

Figure 2.1 shows the magnitude and the phase of the first harmonic, a_1, as a function of time. The three subplots correspond to various values of the damping ratio, $\zeta = \frac{\sigma_k}{|\sigma_k + i\omega_k|}$. The model predicts that the damping ratio goes to zero as the compressor mass flow is reduced. The assumption is that the first three harmonics can sufficiently describe the wave both in amplitude and in phase. The magnitudes of the three first Fourier coefficients are indications of the wave strength, and they increase as the compressor approaches the point of instability. As the waves get stronger their rotating patterns emerge through the noise as a more coherent traveling. In other words, according to the linear model, the phase of the complex coefficients shows larger intervals of uninterrupted traveling as the damping ratio goes down. As one can see from the plots,

the damping is very low (0.02) before the traveling phase patterns are coherent (i.e., before the phase plot is a straight line). Keep in mind that in the case of the ideal-model situation the interference of the noisy compressor environment on the sensors remains unaccounted for. The corrupting effect of compressor noise on the sensors' readings is "enormous"; of amplitudes often greater than those of the perturbations. This is something to remember during the presentation of the results.

Figure 2.2 is a different representation of the same results. It shows the *Power Spectral Density* (PSD) of $a_1(t)$, for the same time histories that were plotted in Figure 2.1. The PSD of a harmonic is the *Discrete Fourier Transform* of the *Autocorrelation* of the Spatial Fourier Coefficients. To that end we calculated the FFT (fast Fourier transform) of the spatial Fourier coefficients (see Brown R.G., 1992) The values of the spatial Fourier coefficients are complex, which means that in general the PSD of the signal takes different values at negative frequencies than it does at positive frequencies. Note that each plot has both the positive and the negative frequency response plotted against each other. The reason for plotting the results this way is to make clear the lack of symmetry about $\omega=0$. The asymmetry makes it possible to distinguish between waves that are standing and waves that are traveling. Standing waves oscillate in amplitude, while traveling waves are of constant amplitude. In a PSD standing waves show no difference between positive and negative frequencies, while traveling waves show asymmetric peaks in the spectrum (Paduano, 1992). The integral of the difference between the positive and the negative frequency response (shaded area in Figure 2.2) makes it possible to quantify, Etchevers (1992), the concept of *traveling-wave energy* in a compressor over a given interval of time. Using the PSD as a detection scheme in the noisy compressor environment is less sensitive to noise than a *differential* scheme such as trying to find straight line behavior of spatial phase plots. Comparing Figures 2.1 and 2.2 makes the

point clear. For the damping ratios of ζ=0.45 and ζ=0.1 the phase plots in Figure 2.1 are inconclusive, while the traveling wave energy is readily identifiable for all runs in Figure 2.2 (for more details see Etchever's, 1992).

At times, however, especially in high-speed machines, where compressibility plays a role, the most notable features of the PSD plots are peaks at integer multiples of the rotor frequency. Actually, the rest of the traveling frequencies are still there, but since the rotor frequency signal is so strong, they are often too small to see on the same scale. Sometimes, this enormous 'rotor' signal is just an artifact of some geometric excitation (like a mass-imbalance vibratory effect on the sensors), and therefore it would appear as a standing wave of extremely large amplitude. In this case the power of the signal remains relatively constant as the compressor goes into stall. It is necessary, therefore, to eliminate such signals from the data in order to see the traveling frequencies. Some kind of narrow-band notch filter is necessary to remove the rotor 'noise' from the data. A feed-forward adaptive LMS approach (similar to Widrow, 1975) is suitable for the task at hand. The advantage of the feed-forward adaptive filter is that it allows wave energy which is uncorrelated to the rotor passage to pass through.

Finally, we used the *integrated wave energy* as a stall warning scheme. In particular, we integrated (calculated the area underneath) the positive and negative power spectra for a certain frequency range. Each compressor is integrated over a different range, since we want to integrate around frequencies that present the strogest traveling. Over the chosen frequency range, we estimated the difference between the positive and negative power for each run. Finally, we normalized the difference by setting the negative power between frequencies 0 and 1 to the value of 1. We did this in an attempt to "normalize out" any increases in the sensor noise levels as the compressors approach stall inception. This normalization is based on the assumption that the sensor noise is white,

and that the negative frequency spectral response of the compressors is relatively flat (i.e. all the system dynamics tend to rotate in the rotor direction). Since an increase in system excitation arguably constitutes a valid stall warning indicator, this approach is conservative.

We repeated the following three steps for the same fixed time windows of 50 rotor revs and for the same frequency range: 1) calculate the PSD, 2) integrate of the area difference, and 3) normalize the area integral. The window size was chosen after testing several window lengths. We had to compromise between long time windows, which tend to average out trends, and short time windows, which tend to yield noisy results. Remember that the raw compressor data is quite noisy, and this noise introduces a high variance in the values of the *integrated wave energy* (the normalized area-difference integral of the PSD). Keep in mind that the smaller the window the larger the variance of the plot.

Having seen the motivation for the various data-reduction procedures, it is time to give an outline of the typical steps of the data analysis:

1. Basic data preparation:
   a) Examine raw data for outliers and anomalies;
   b) Detrend the data to remove any zero or very low frequency variations;
   c) Normalize root mean square fluctuations across the circumferential array to take out effects of miscallibration and sensor positioning.
2. Calculate spatial Fourier Coefficients (for example, 8 probes $\Rightarrow$ spatial Fourier coefficients 1,2 and 3 using eq. (2)); plot phase and magnitude as functions of time.
3. When necessary, eliminate oscillations which are highly correlated with the rotor rotation rate (feed-forward adaptive LMS algorithm), or local to a few sensors.

4. Calculate power spectra of the pre-stall data; plot and compare positive and negative frequencies. Plot the time history of the PSD of the positive frequencies for the first harmonic.

5. Compute integrated area difference between positive and negative frequency spectra.

Since plotting every single result of the above procedure, for every compressor, would fill a substantial volume, this thesis will only try to summarize common trends and characterize each compressor with respect to the current model of pre-stall compressor dynamics.

3. DATA ANALYSIS RESULTS AND DISCUSSION

This is the central chapter of this thesis, and it includes all the results of the data-reduction procedure, as presented in chapter 2, on most of the runs of all the 9 compressors. Following is a list of sections and short descriptions of each one:

- Stall Inception Transients — will concentrate on plots of the raw data and of the spatial Fourier coefficients in the stall-inception region.
- Pre-Stall Power Spectra — will concentrate on PSD plots in the pre-stall region.
- Rotating Wave Energy and Compressor Stability — will center on time histories of PSD plots.
- Wave Energy as Stall Warning — will focus on plots of the integrated wave energy vs. time.
- Wave Energy strength with respect to axial location an corrected speed — will focus on plots of the integrated wave energy vs. stage and corrected speed.
- Discussion — a discussion of the results.

I STALL INCEPTION TRANSIENTS

This section has only raw data without absolutely no reduction. The data of Figure 3.1 of the results are the pressure readings of the circumferential sensors for about the last 30 rotor revolutions before stall. There are stall-inception data from all 9 compressors. The scales have been altered to allow a qualitative comparison of trends and to emphasize the similarities between the tests. The data that follows is for the highest rotational speeds, that were available; usually 100% of the design speed. The reason for presenting the 100% speeds is that at high rotational speeds, the compressors are more likely to end in one-dimensional surge. Therefore, it makes sense to show that rotating disturbances exist in all compressors at the highest speeds available. Even in cases where the compressor finally goes into surge, there is a period over which the instability is two-

dimensional stall. Although not shown here, over 30 runs at various speeds, at different stages and compressors have been investigated for this thesis. Rotating, two-dimensional perturbations exist in every case studied, even in those instances where the compressor surges.

Of all the compressors in Figure 3.1 only #1 and #8 end up in fully developed rotating stall, while the rest go into surge. Note that the transients that follow the surge event in some runs are due to the opening of the throttle valve, so that the compressors can recover and avoid mechanical damage. As forementioned, whether the compressor flow develops into a one- or a two- dimensional limit cycle, rotating stall, and not surge, is what sets the performance bounds in axial compressors. In other words, if one is to improve the performance of an axial compressor by eliminating its instability modes then he should eliminate stall first. Eliminating the surge mode alone would be of no advantage to the performance of the system, since stall would still occur. Greitzer et al. (1978) showed the latter statement to be true on a low-speed machine.

The plots of compressors #1 and #5 in Figure 3.1 give good examples of the pre-stall, the stall-inception and the fully-developed-stall regions. The rest of the compressors surge at the end, and thus they give examples of what we will call the pre-stall, stall/surge inception and surge regions. The difference is that although the stall cell appears initially, it actually never grows into fully developed stall.

Going one step further on the data-reduction ladder, the data was decomposed into their spatial harmonics as described by Eq. (2) of Chapter 2. The task of detecting traveling waves in the raw data could be done by looking for traveling patterns within the noisy pressure data. This approach of using the SFCs is a little bit less cumbersome than looking at the raw data. The plotted results of Eq (2) make it easier for us to see traveling of small amplitude perturbations. Furthermore, at this stage, one cannot really tell the time behavior of the rotor frequency pulsation, nor whether it is a result of the system's dynamics or just unwanted noise. We decided, therefore, to eliminate the intense

rotor signal from the data. Doing so allows us to see whether other frequencies travel around the annulus, and whether they increase in strength as the compressor becomes more and more unstable. According to the discussion in Chapter 2, the traveling frequencies will manifest themselves in the time histories of the phase plots of the spatial Fourier coefficients as straight-line segments of slopes equal to the strongest frequency. One might expect that the slope of the phase plot during the instability would be the same as that just before the initiation of the event. In fact, one would expect not just the same slope but also the same straight line extending from the inception section and even from the pre-stall region all the way into the mature event.

The scenario just described occurs under idealized conditions. Unfortunately, the behavior of real machines is much more complex. As mentioned in Chapter 2, the noise levels in the compressor environment are of magnitude comparable of that of the signals (of the order of 0.01 psi). In addition, the sensors lacked the sensitivity to grasp well such small signals (50-100 psi sensors). The reason for the sensors' inadequacy is that they are quite expensive, and therefore, they must be designed to withstand the high-pressure vibrations that occur when the compressor becomes unstable; not to mention the high temperatures of the order of 500 °F. The end result of such compromise is: having 100 psi sensors to try to measure signals of the order of 0.01 psi. The sensors' shortcomings, in addition to the relatively high levels of noise, make model-data inconsistencies quite understandable. Keeping all these comments in mind, one can have a better understanding of the of the plots in Figures 3.2 and 3.3.

Figure 3.2 presents the time histories of the first two spatial harmonics (a_1 and a_2) of all the 100% runs that were shown in Figure 3.1. After the rotor frequency has been filtered out, the traveling waves can be detected for most of the runs of the compressors studied. There are straight-line segments in the phase plots, and their slope represents the rotational speed of the waves. Note that the straight-line sections are not continuous; they are often interrupted by random noise. Many times the slope of the phase of the waves is

the same as that of the final event. To see this compare the slopes of Figures 3.2 and 3.3 to the data of Table 1. Figure 3.3 shows similar plots to those of Figure 3.2 for those compressors for which the 70%-corrected-speed run was available. Clearly, at this lower speed the waves appear in coherent patterns for a longer time than at 100%.

Having established the fact that traveling waves exist, and that they can be identified through the slope of the phase plots, it is a natural question to ask whether this scheme can be used as a stall warning scheme. Stall warning could be used in a control scheme that would either passively (reduce the fuel supply, open the throttle, etc.) or actively (reposition guide vanes, blow air into the compressor flow, etc.) avoid stall initiation. To avoid stall implies to improve the performance of the system, as well as to extend its life, since high-pressure vibrations during stall could cause severe structural damage. Therefore, the feasibility of an avoidance scheme, that uses traveling waves as stall precursors, depends on the ability of the detection method of triggering the waves some time before the event. This way the active control scheme must have sufficient time to counteract the effect of time delays and to prevent the instability. Our attempts to design such a scheme included calculations of the rotational speed of the SFCs. Speeds that would remain within certain range ($\pm 10\%$ of some value) for enough time (in the order of 10 rotor revolutions) would set off the warning. Unfortunately, such warning scheme did not work because the data is very noisy, and the phase becomes incoherent.

If before stall initiation, the 'wave' is consists of many approximately-of-equal-strength frequencies, the phase of the Fourier coefficients will lose its coherence. Something similar appeared in the simulation results shown in Chapter 2 (for damping ratio ζ=0.45). As one can see on Figure 2.2a the frequencies between ω=0.15 and ω=0.35 are of comparable strength. Looking at the phase plot of that same signal (Figure 2.1a) we can see a behavior similar to that seen in, for instance, Figure 3.2, compressor 4.

The phase-slope approach to stall warning is very conservative, since, as shown in Chapter 2, the damping of the system has to be quite low before the system behaves as

anticipated (continuous straight line segments in the phase plot). Besides, in the actual run the relatively high noise level is expected to cause the data to digress from the model predictions; not to mention the lack of sensitivity of the sensors. Last but not least, as shown by Mansoux (1993), nonliner interaction between modes during stall inception often causes energy to be transferred between the spatial harmonics. This may cause certain harmonics to weaken while other harmonics grow. During the period when a certain harmonic is small, the relatively high noise combined with the nature of the non-linearity can cause its phase to wander.

Keeping in mind the details just mentioned, stall-warning time estimates can be extracted from the plot of Figures 3.2 and 3.3. The warning time is the time over which we can trace the same straight line back into the pre-stall zone on *either* of the first two harmonics. According to this scheme, in Figure 3.2, the waves in the compressors 1, 2, 3 and 9 are quite strong, and they can be traced all the way out, into the pre-stall domain. However, in the same Figure 3.2, compressors 4, 5, 6, 7 and 8 show either very small or no warning. In the former cases there is no question that pre-stall traveling waves exist. It can also be argued that waves are indeed the cause of the instability. In the latter compressors, although traveling is evident due to the small straight line sections, we can not prove from this data that they cause the compressor to become unstable, since their straight-line path is interrupted.

Looking further, one can see that there is traveling in compressors 6 and 8. The traveling in these cases is different in nature from what was described earlier. It evolves in a 'stair-step' fashion instead of a straight line. In addition to those two, compressor 2 also exhibits stair-step traveling, as well as some traveling in a direction opposite to the rotor rotation; we will refer to such traveling as 'negative traveling' as opposed to 'positive traveling' in the direction of the rotor rotation. Boussios (1993) showed by simulations that such behavior is typical of compressors operating in distorted flow.

Figure 3.3 shows traveling in all the 70% cases. In these plots the traveling waves are strong. We can see from the plots that their amplitude is quite high (although much smaller than the amplitude of the full grown event). Their phase is more coherent than the 100% cases, and therefore, we are able to trace the straight-line traveling well into the pre-stall region. Consequently, the warning times are longer compared to the runs of Figure 3.2.

II PRE-STALL POWER SPECTRA

In the previous section we investigated the approach of using the phase of the spatial Fourier coefficients for detecting traveling waves in the data. Unfortunately, both the detection scheme and the warning scheme are very sensitive to the relatively high level of sensor noise. This high sensitivity of the phase to disturbances makes the approach inadequate for some of the runs in Figure 3.2.

To try to overcome the interference of the aerodynamic and mechanical vibrations, a judicious practice would be to transfer the analysis to the frequency domain. In other words, instead of looking for a single dominating frequency that lasts for a 'long time', we can sum up all the bits and pieces of every frequency over a fixed time period and then consider those which have the highest 'sums'. To say it in more scientific terms calculate the Power Spectra of the spatial Fourier coefficients. Our task has now changed; instead of looking for deterministic waves around the annulus, we concentrate on the existence of *stochastic* traveling waves.

The power spectra are representations of how much power (energy per unit time) of each frequency there is in the signals. Of course, as we discussed in Chapter 2, what is important is the difference in the power between the positive and negative frequencies. Recall that if the positive and the negative representations of the same frequency are equal then we have just a standing wave; otherwise we have a traveling wave. A nice feature of

this approach is that white sensor noise appears only as a flat vertical displacement in the plots as shown.

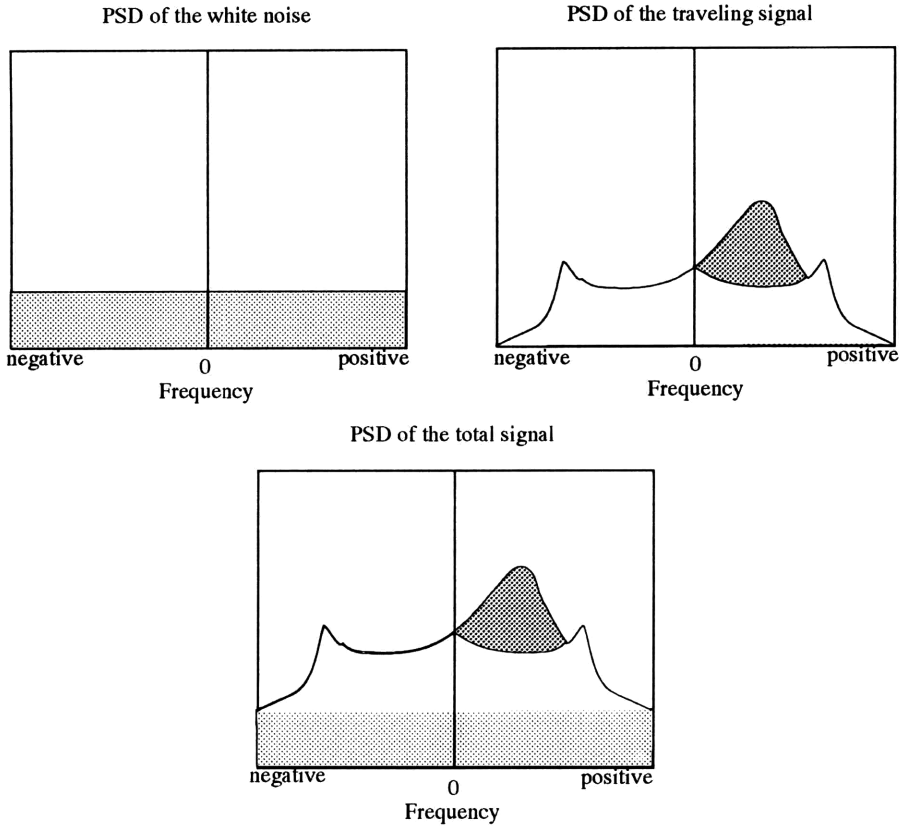

Consequently, assuming that the sensor interference is white, the area difference between the positive and the negative frequencies is a quantitative representation of the traveling-wave power. This area difference is a gauge of the amount of spectral power that is traveling relative to what is standing. We shall call the area difference 'traveling wave energy'.

It makes sense at this point to calculate the power spectra for the runs that were seen in Figures 3.2 and 3.3. If the discussion above is correct then we expect the power spectra to answer a lot of the questions. At this point, since we have no reason to believe otherwise, the rotor frequency signal is filtered out as noise. In the next section, however, we will see that in fact the rotor frequency signal can be an important indicator of the dynamics of the system. Figures 3.4 and 3.5 show the power spectra of the data of Figures 3.2 and 3.3. The nondimensional time window over which the PSDs were

calculated was kept the same in all cases (approximately 100 rotor revs). The vertical scales of the plots do not carry any quantitative significance, since for each run the readings of the pressure transducers scaled to a voltage through various transforming constants which often were not provided. Keep in mind, also, that the time windows involved in the calculations of the power spectra end just before the stall-inception point. Thus the power shown is from within the pre-stall region.

The spectra indicate that the runs of Figures 3.4 and 3.5 have a significant amount of traveling for at least the last 100 rotor revolutions. The shaded peak in a spectrum indicates a wave rotating around the compressor annulus at the designated frequency. The wavelength of the traveling signal is the compressor circumference divided by the spatial-harmonic number (k). Note that compressors 3, 6 and 7 of the 100% cases and 1 and 2 of the 70% cases display a behavior very similar to the model simulation of Chapter 2. In these runs all the traveling energy is within a narrow frequency range; yet not quite as narrow as one would expect from Figure 2.2. Also, notice that the frequency of the second spatial harmonic is twice that of the first. Such a result is in agreement with the simplified model of the last chapter. However, for compressors 2, 4, 5 and 8 of the 100% runs and 4 and 7 of the 70% runs, the trend is different. Although there are indications of traveling in these cases, the appearance of the PSD's differs from the third plot of Figure 2.2. The waves here have broad spectra. Some of the runs (for instance #7 of the 70%) look like Figure 2.2 for ζ=0.45. This could be evidence that, during the pre-stall section, the system stays most of the time at a damping ratio that is quite high. Then, just before and during stall inception, the damping ratio drops rapidly to near zero, and the compressor becomes unstable. In other cases, i.e. compressors 2 at 100% corrected speed, the spatial harmonics show more than one frequency (mode). In fact, in many cases the frequency content of the harmonics seems to be multiple, which implies that more than one eigenvalues is involved in the stall-inception process. Note, especially,

compressors 4, 5 and 8 of Figure 3.4. Their spectra are very broad, which accounts for the lack of any coherence in their phase plots in Figure 3.2.

III ROTATING WAVE ENERGY AND COMPRESSOR STABILITY

In the two sections that preceded we established a confidence that traveling waves do indeed exist in all the compressors studied. We assumed in the analysis that these waves can be spatially decomposed into harmonics. Furthermore, we assumed that two or three of these spatial harmonics can effectively reproduce the wave; theoretically we need infinitely many of these spatial harmonics to exactly reproduce the original wave. Each harmonic was viewed as an independent state of the system. Therefore, there is at least one eigenvalue associated with a particular harmonic. The eigenvalues of each harmonic manifest themselves as spikes of area difference in the spectra of that particular harmonic.

At this point it is important to remember that the system is changing dynamically during the closing of the throttle. The transfer function that represents the system, with all its poles and/or zeros, is changing as the throttle position changes. We assume that, since the throttle motion is continuous, the pole-zero locus of the system will also be continuous. On the other hand, for the small time interval of the PSD (about 100 rotor revs) we had to assume stationarity, which means that the system dynamics are not changing, or that the change is so small that it can be ignored.

Thus, it makes sense to observe the system dynamics as the compressor goes into stall. A time history of the power spectra provides exactly what we need. Since we want the total transfer function of the system, we will not bother to eliminate any signal from the data (i.e. rotor frequency noise). Assuming that the excitation of the system is not changing as the throttle closes, any artificial or localize effects (such as mass imbalance vibrations) would only appear in the plots at a constant level. The power levels, however, of the traveling frequencies are expected to rise as the damping of the system goes to zero.

For some of the compressors (those for which we had data from open throttle position all the way into stall) we created 3-D waterfall plots. This plot gives a convenient way to visualize the compressor dynamics as they evolve over time. In the Figures 3.6, 3.7, 3.8, 3.9, 3.10, 3.11 and 3.12 we show time histories of the power spectral densities of compressors 2, 4, 5 and 8 for the positive frequencies. Most of the analysis was done for compressor 4 because this was the one for which the most complete information was available. The time length of each individual spectrum was taken to be 50 rotor revs. The choice of 50 rotor revs for the time length was chosen to keep the assumption of stationarity (i.e. the system dynamics remain unchanged over the time interval) valid and still achieve a reasonable resolution in the frequency plot. Spectra are calculated as the time window advances through the data in a point-by-point fashion. Keep in mind that the time window starts 50 rotor revolutions in the past and ends at the present time.

Figure 3.6a shows one of the runs of compressor 4 at 70% corrected speed taken along its characteristic from the open throttle condition to the fully-developed-stall region. In the plot one can easily identify the rotating stall frequency of about 70% of the rotor speed. Although it seems that there is no traveling before stall, this is not the case. Actually, the traveling becomes visible if we replot the same power spectrum history in just the pre-stall region. This time the vertical scale is about 50 times smaller. In this setting (see Figure 3.6b) traveling is very clear. In fact, it exists for more than 1000 rotor revs before the instability. We can primarily distinguish 2 frequencies, at 70 and 100% of the rotor frequency. Notice that the peak at the shaft frequency is the strongest. Also, notice that it seems as if the 70% and the 100% peaks are beating against each other, perhaps due to some nonlinear intermode coupling. Whenever the strength of the rotor frequency goes down, the power content of the 70% peak increases. Finally, note the appearance of a peak at 50% of the rotor frequency just before stall inception. Once the stall inception process starts, it is the peak at 70% of the rotor frequency that goes into stall.

The behavior of compressor 4 is a strong function of its corrected speed. Figure 3.7 includes the waterfall plots for compressor 4 for various shaft speeds. Notice that the strength of the once per rev is increasing as the shaft speed increases. In all cases both the 70% and the 100% signals are present. However, at the 100% corrected speed the 70% signal is about 200 times weaker than the rotor signal, as compared to about 6 times smaller in the rest of the runs. At all 6 speeds shown the rotor frequency signal is not only the strongest, but it also seems to be the one that is leading the system to the instability. Figure 3.8 is the same as Figure 3.7 except that four runs are shown on the same scale. Although, from the 70% run to the 80% run, the peak value of the rotor-frequency power actually drops, the general trend is that higher speeds have stronger rotor-frequency peaks. If we assume the system is linear, Figures 3.7 and 3.8 indicate that the there is a system pole near the rotor frequency and one near 70% of the rotor speed, and that they both approach the imaginary axis. The 100% pole seems to be the closest to the $j\omega$-axis for most of the time, but in the end, as the damping of the system approaches zero, the 70% pole becomes unstable first.

The waterfall plots just described seem to provide insight into the form of the data and trends with the rotor speed and throttle position. Thus we consider it worthwhile to make waterfall plots for the rest of the runs, or at least for those runs that we have transients from open throttle to stall. The results appear in Figures 3.9 through 3.12. Figure 3.9 shows the waterfall plots for the 1-stage Military fan (compressor #2), Figure 3.10 analyzes the 5-stage core compressor (compressor #5), Figure 3.11 the T55 axi-centrifugal (compressor #7) and Figure 3.12 the Viper Engine (compressor #8). We will discuss each in turn.

Looking at Figures 3.9 and 3.10 in more detail, we can see that compressors 2 and 5 behave in a manner very similar to the 4-stage (Figures 3.7 and 3.8): at 100% corrected speed the rotor signal seems to be the most lightly damped until stall initiation when the system becomes unstable at an instability frequency of 50% (see Table 1). In the 70%

cases the 50% poles seem to be the most lightly damped poles all through the transient from the pre-stall region to the instability. The rotor frequency pole in these runs, if any, seems to be far from the imaginary axis. In fact, it seems to be farther away from the jω-axis in compressor 2 (Figure 3.9), while it seems non-existent for compressor 5 (Figure 3.10).

The data of the T55 (compressor #7, Figure 3.11a) is different in the sense that the throttle closed very slowly, and therefore, for a comparable time scale (in rotor revs) there was not any significant change in the strength of the rotor signal or any other discernible frequencies. Figure 3.11b shows the 1000-rotor-rev time history of the power spectra of the two 7-stage runs; 70% and 100% corrected speed. Figure 3.11b shows spectral histories for a frequency range from 0 to about 10 times the rotor frequency. Unfortunately, these do not indicate any trends that enhance our understanding of the data.

Since the throttle closing rate for the T55 (compressor #7) was very low, we decided to try to simulate a waterfall plot like those of compressors 2, 5 and 8 by creating a three-dimensional power spectra plot that consists of just three points (Figure 3.11c). The three PSD's used for these plots were taken along the same speed line, with the throttle almost stationary in all three cases. The "time" axis is roughly scaled to reflect the flow coefficient of each spectrum. After taking the data at the first two steady state points before stall, we closed the compressor very slowly to stall to get the data shown in Figures 3.11a and 3.11b. The throttle change during the transient is so tiny that it makes no difference on the map. Under these circumstances Figures 3.11a and 3.11b do not show the real story about the T55. In Figure 3.11c, on the other hand, indicates that the rotor frequency dominates the signal and grows as the stall point is approached. We conjecture that this peak is causing the system to stall. The behavior of the T55 falls within the expectations set by compressors 2 and 5.

Figure 3.12a is the Viper Engine data (compressor 8). This case is different from the other compressors in that it is not a compressor but a real engine. However, the waterfall behavior of this machine is very similar to the T55. Note that at both the 81% and the 98% runs the rotor signal dominates the data. In the 81% case the once-per-rev signal suggests the rotor-frequency pole to be the most lightly damped pole, and it becomes less damped as the compressor approaches stall. On the other hand, in the 98% run, the rotor signal does not grow in strength over time; at least not enough to become apparent. If we look at the waterfall plots over wide frequency range (Figure 3.12b), we can recognize signals of 6 times the frequency of the rotor to increase slightly as the engine approaches stall. This trend appears strong in the 98% run. The 81% run, on the other hand, does not show any significant trends on Figure 3.12b; just a slight increase of the twice-per-rev signal. Figure 3.12c. This is another waterfall plot of the 81% run of the Viper Engine. This time, though, there is a clear traveling trend leading the compressor to stall. The reason we did not observe the same trend earlier is because Figure 3.12c is a visualization of the power spectra history of the *second* spatial Fourier coefficient. We see two major peaks; one on each plot. The positive peak is at a different frequency than the negative, which suggests poles at both positive and negative frequencies. Since compressor 8 has only 4 sensors, we lose the phase information of the second SFC when we decompose the signal into its spatial harmonics. Thus it was necessary to plot the waterfalls of both the positive and the frequencies to verify that the peaks indicate traveling waves.

IV WAVE ENERGY AS STALL WARNING

From the results presented in section III, it is very clear that the pre-stall and the stall-inception processes are accompanied by an increase of the power of certain frequencies. Therefore, it makes sense to use this trend somehow in a stall-warning scheme. In the five particular study cases of compressors 2, 4, 5, 7 and 8, at the 100%

corrected speed and most of the other shaft speeds, that frequency was the rotor frequency. However, in some runs (i.e., 70% compressor 2) other frequencies led the compressors to the instability.

The concept of the power spectrum was the one that lead us to the results of the previous section. Recall that the area between the positive and negative frequencies is an indicator of wave traveling power. The results of section III imply that the energy or power of the compressors jumps as they approach stall.

Figure 3.13 is an implementation of the ideas above for compressor #4. In Chapter 2 we gave a step by step description of the process. The choice of the frequency range was made after we looked at the results of part II and III; each compressor is integrated over a different range. For instance, for the Viper Engine at 100% corrected speed, the best range would be around 6 times the shaft speed. For the 4-stage machine, the frequency range that was chosen was between 25% and 125% of the shaft speed.

For Figure 3.13 we marched the fixed time window over the data stream for four shaft speeds. For the 70%, 75%, 80% and 100% runs shown on Figure 3.13 the throttle closing rate was kept the same. The data is aligned in such a way that the stall initiation point is matched to the 0 time for all the runs. This makes the comparison easier. Notice that in all the cases of Figure 3.13 the integrated wave energy rises steeply at 100-200 rotor revolutions prior to stall. The mean d.c. level of the of the integrated energy remains almost constant for the 70% and 75% speeds until the pre-stall rise occurs. The 80% case is different in that the d.c. level drops for about 1000 rotor revolutions prior to stall. This case is unique in that sense, since it was the only one behaving in this manner. The 100% run shows slow rise of the d.c. level all along until the more aggressive jump of the pre-stall rise. For some corrected speeds we had multiple runs at similar conditions. These runs show different values for the time of the pre-stall warning rise. Of all the runs we show the ones with the smallest pre-stall rise.

Figure 3.14 is an expanded scale version of the plots of Figure 3.13. The plots of Figure 3.14 show the threshold needed to use this method as a warning scheme. The choice of such threshold requires care since the integrated-energy time trace is very noisy. The approach of choosing the threshold in this case was a very simple one; we chose the threshold to be just higher than the highest peak observed before the 200th rotor revolution prior to stall. The warning that results from such scheme is of the order of 100 to 200 rotor revolutions even for the 100% case. For conditions for which we have multiple runs, we show the ones with the smallest pre-stall rise. The warning times indicated in Figure 3.14 are rather conservative and we could probably improve the results using additional signal processing. For instance, removing the high frequency spikes or incorporating the low frequency d.c. level changes would probably increase the reliability of the warning time considerably.

Since the throttle closure rate was constant during any single test run and the pressure rise and mass flow were measured, the operating point along the speedline at the time corresponding to the stall warning period would be determined. At the 100% speed the warning time was equivalent to about 0.2% change in mass flow. Data was analyzed for the 100% speed for various throttle closure rates. Those rates varied by a factor of thirty (the rate, however, was kept constant during each test). The data of all these runs behaved in a similar manner. That is to say that the d.c. level of the integrated energy rose slowly in all of them until a more abrupt rise just prior to stall initiation. The level correlated with operating point on the speedline so that amplitude of the wave energy was found to be high for proportionally longer period at low throttle rates than at higher ones. For compressor #4, at least, the level of wave energy is clearly a function of the position along the speedline.

Overall, these results are very encouraging. They show that traveling wave energy can be used to identify pre-stall waves in high speed compressors, even at the highest rotational speeds and throttle rates - conditions at which study of the spatial Fourier

coefficient time histories has proven unreliable. Furthermore, increased wave energy is discernible for a significant amount of time (of the order of 100-200 rotor revolutions) before stall in all runs. More work, however, needs to be done in the area of signal processing for such scheme to be considered reliable in stall warning.

V WAVE ENERGY STRENGTH WITH RESPECT TO AXIAL LOCATION AND CORRECTED SPEED

Having established a ground for a stall warning scheme it makes sense to try to create a locus of the wave energy as a function of both the axial location and the corrected speed. Such an attempt might give us a better way to position our sensors so that we get the best sensitivity out of them in the future. Figure 3.15 does just that. The plot shown is created for compressor #4. The values on the vertical scale are equal to the wave energy difference between positive and negative frequencies normalized by twice the negative frequency traveling (this will conservatively account for the change in the sensor noise and allow a percentage comparison between different runs). We had data only for stages 1, 2 and 4. Notice that the wave energy count (as defined in the previous sentence) is maximum at stage 2. If, however, we remove the rotor signal from the data, the most wave energy traveling can be detected in stage 4. Figure 3.16 shows the integrated wave energy, but after the rotor frequency signal and its harmonics have been eliminated. This means that there is more traveling wave energy (at frequencies other than the rotor frequency) in this stage than in any of the other stages for which we had data. This is why the data of compressor 4 shown earlier are taken from stage 4.

VI DISCUSSION

It has been apparent throughout the result section that the machines examined behave in a similar manner. They all first develop a two-dimensional rotating instability (rotating stall) regardless of whether or not they finally surged. Moreover, their behavior

in the small amplitude pre-stall region is indicative of multi-mode, oscillatory, dynamic systems. This behavior has implications in the compressor design that need to be discussed.

The results of the linearized theory of Moore and Greitzer were developed for small amplitude perturbations and they are valid in the pre-stall region. However, during stall inception the size of the waves becomes significantly larger as they evolve into stall. Obviously, the linearized theory will not work under these conditions. Nor would it be appropriate to use this model to describe the dynamics of a part-span rotating stall found in some compressors prior to surge or large amplitude stall. The reason the model is not valid in these regions is that the assumption that ~~the~~ each spatial harmonic and each mode evolve independently is no longer true. This is seen in the runs of compressors 2, 4, 5, 7 and 8 where the signal at the shaft frequency evolves into other signals of frequencies equal to fractions of the shaft frequency. This evolution is through some nonlinear mode coupling which the linearized model is unable to predict.

In addition, the assumption that the flow can be described by a two-dimensional model can be limiting. In particular, low hub-to-tip compressors, like compressor 1, tend to develop three-dimensional flow. The addition of a third spatial dimension brings to the picture additional resonant modes. Although, in the compressors studied, a two-dimensional mode goes unstable it would certainly be possible that a three-dimensional mode is the most critical in some other compressor.

In the past, researchers focused their attention on fully developed stall and surge or on the stall inception process. It is, however, the pre-stall region which is the most interesting for designing a stall avoidance scheme. In many ways the fluid dynamic stability of a compressor can be viewed in a way similar to its structural dynamic stability. In both cases the compressor is a system rich in closely spaced, orthogonal modes operating in the presence of a strong forcing. As shown by Tryfonidis, et al. (1994) many modes can exist simultaneously, and which mode limits the compressor stability is a

function of operating point and performance characteristics. Besides, it can also be seen in the several waterfalls of the result section that two or more modes may have very low damping simultaneously. The stability of the compressor may thus be set by the influence of the external forcing on the modes, which is beyond to scope of linear theory. The slope of the speedlines, and thus the damping of the mode, is very hard to estimate. However, the influence of geometry changes on the compressor stability is often useful in design, and it can now be assessed. For example, the modeling indicates that the modal damping is sensitive to axial loading. Or, reduction of losses, blockages and deviation help to increase speedline slope and consequently increase stability.

Forcing of the modal structure is an important consideration for overall compressor stability. Compressor dynamics like those described in this thesis can go unstable if the forcing has sufficient amplitude. With the exception of inlet distortion the perturbation structure in compressors has not been studied in the context of compressor stability. It is therefore very difficult to characterize a particular machine as being weakly or strongly forced. It is clear however, that the noisy pressure signal in the compressors is often dominated by the shaft-frequency signal which reaches up to several percent of the mean flow. Manufacturing non-uniformities as well as non-uniformities of tip clearance may influence this forcing and therefore, affect compressor stability.

The system dynamic response to forcing can be studied analytically. Even in the case that the damping ratio is quite high (positive), and thus the linear stability of the system is not yet threatened, the wave strength can be large enough to trigger a nonlinear response of the system.. In this case the nonlinear stability of the system, or resistance to perturbations, is at risk. Mansoux et al. (1993) have developed a Lyapunov stability analysis of the Moore-Greitzer model in an attempt to accommodate such occurrences. In particular, when the domain of attraction of the operating point becomes very small, perturbations that are safe in the linear sense can actually force the system to the instability through nonlinear effects. It is, therefore, a combination of the low damping, as well as

the increased forcing and the weakening of the nonlinear resistance to perturbations that determines that rotating stall inception point.

Finally, it is important to keep in mind that the pre-stall signal consists of more than just one spatial harmonic. In some of the compressors studied, rotating stall consists or two or more stall cells. Compressors 1, 3, 5 and 6 exhibited very strong second harmonic in the results of Figures 3.2, 3.3 and 3.4. Note that higher harmonics travel at the same speed as the first harmonic, and, therefore, are also affected by the same forcing.

Another concern is the short length scale disturbances reported in the Viper engine by Day and Freeman, and by Day in low speed compressors, which may also play a role in stall inception. These may be either a three-dimensional response of the system or some system forcing which triggers stall. Unfortunately, the data analysis techniques that were used here are not suitable for detecting the short length scale disturbances since their energy would be spread across many spatial harmonics.

4. SUMMARY AND CONCLUSIONS

This thesis includes data from nine compressors that come from four different manufacturers and represent a wide range of approaches to compressor design. There are core, fans and engine compressors at various hub-to-tip ratios, stages and loading. There are, however, certain characteristic that appear in all of them, and they were the focus of this thesis.

In particular, we have shown that stall precedes surge in all of the compressors tested. Although many researchers reached the same conclusion independently in the past it is useful to validate the result among a wide range of different compressors. Further, we investigated several techniques for the detection of small amplitude traveling waves. We determined further the limitations of each approach. The old tool of power spectra of the spatial Fourier harmonics is utilized in a different, new way. Using the new tool we have shown that:

1. Low amplitude traveling waves are found in all of the compressors prior to stall.
2. The traveling wave structure is different at low and high corrected speeds. Specifically, a wave rotating at a fraction of the shaft frequency grows strongly at low speeds, while a shaft frequency disturbance dominates at 100% speed.
3. At constant speed, the wave structure is a function of the position on compressor speedline.

The concepts developed through the analysis and the data reduction led naturally to the idea of "integrated traveling wave energy" as a measure of compressor stability. We showed that the wave energy is a function of the operating point on the speedline. Further, for the cases that we tested under this new idea we found a warning time of the order of 100 rotor revolutions. There is sane evidence that further refinement of this approach can turn it into a reliable warning scheme.

Finally, we demonstrated that wave energy varies from stage to stage in the same compressor, and it is definately a strong function of corrected speed.

References

Boussios, C.I., 1993, "Rotating Stall Inception: Nonlinear Simulation, and Detection with Inlet Distortion," M.S. Thesis, MIT Dept. of Mechanical Engineering, February.

Bonnaure, L.P., 1991, "Modeling High Speed Multistage Compressor Stability," M.S. Thesis, MIT Dept. of Aeronautics and Astronautics, September.

Boyer, K.M., King, P.I., Copenhaver, W.W., 1993, "Stall Inception in Single Stage, High-Speed Compressors with Straight and Swept Leading Edges," AIAA 93-1870, presented at the AIAA/SAE/ASME/ASEE 29th Joint Propulsion Conference and Exhibit, Monterey, CA, June 29-30.

Brown, R.G., Hwang, P.Y.C., 1992, "Introduction to Random Signals and Applied Kalman Filtering," second edition, Wiley, pp. 121-125.

Day, I.J., 1993a, "Stall Inception in Axial Flow Compressors," *J. of Turbomachinery*, Vol. 115, No. 1, January.

Day, I.J., 1993b, "Active Suppression of Rotating Stall and Surge in Axial Compressors," *J. of Turbomachinery*, Vol. 115, No. 1, January.

Day, I.J., Freeman C., 1993c, "The Unstable Behavior of Low and High Speed Compressors," presented at the International Gas Turbine and Aeroengine Congress and Exposition, Cincinnati, OH, May 24-27.

Emmons, A.W., Pearson, C.E., Grant, H.P., 1955, "Compressor Surge and Stall Propagation," *Trans. of ASME*, Vol. 79, pp. 455-469, April.

Etchevers, O., 1992, "Evaluation of Rotating Stall Warning Schemes for Axial Compressors," M.S. Thesis, MIT Dept. of Aeronautics and Astronautics, August.

Freeman, C., Wilson, A.G., 1993, "Stall Inception and Post Stall Transients in an Aero Engine Axial Flow Compressor," presented at I. Mech. E.

Gallops, G.W., Roadinger, T.J., French, J.V., 1993, "Stall Testing and Analysis of Two Mixed Flow Turbofans," ASME paper 93-GT-62, presented at the International Gas Turbine and Aeroengine Congress and Exposition, Cincinnati, OH, May 24-27.

Garnier, V.H., Epstein, A.H.,Greitzer, E.M., 1991, "Rotating Waves as a Stall Inception Indicator in Axial Compressors," *J. of Turbomachinery*, Vol. 113, April.

Hendrics, G.J., et al., 1993, "Analysis of Rotating Stall Onset in High-Speed Axial Flow Compressors," AIAA paper 93-2233, presented at the AIAA/SAE/ASME/ASEE 29th Joint Propulsion Conference and Exhibit, Monterey, CA, June 29-30.

Hoying, D.A., 1993, "Stall Inception in a Multistage High Speed Axial Compressor," AIAA paper 93-2386, presented at the AIAA/SAE/ASME/ASEE 29th Joint Propulsion Conference and Exhibit, Monterey, CA, June 29-30.

Mansoux, C., Gysling, D.L., Paduano J.D., 1994, "Distributed Nonlinear Modeling of Axial Compressor Stall and Surge," to appear, *Proc. of 1994 American Control Conference*, Baltimore, June.

McDougall, N.M., Cumpsty, N.A., Hynes, T.P., 1990, "Stall Inception is Axial Compressors," *ASME J. of Turbomachinery*, Vol. 112, pp. 116-125.

Moore, F.K., Greitzer, E.M., 1986, "A Theory of Post-Stall Transients in Axial Compression Systems, Part I - Development of Equations, and Part II - Application," *ASME J. of Engineering for Gas Turbines and Power*, Vol. 108, pp. 68-97.

Owen, A.K., 1993, "Analysis of the Rig Test Data for an Axil/Centrifugal Compressor in the 12 Kg/Sec Class," presented at AGARD 82nd PEP, Montreal, Canada, October.

Tryfonidis, M., et al., 1994, "Pre-Stall Behavior of Several High-Speed Compressors," to appear, *Proc. of 1994 ASME Turbo Expo*, The Hague, Netherlands, June.

Paduano, J.D., 1992, "Active Control of Rotating Stall in Axial Compressors," Ph.D. Thesis, MIT Dept. of Aeronautics and Astronautics, February.

Widrow, B., 1975, "Adaptive Noise Canseling Principles and Applications," Proc. IEEE, Vol. 63, December, pp. 1692-1716.

Compressor	70% runs		100% runs	
	Pre-Stall	Fully Developed	Pre-Stall	Fully Developed
1	--	--	45%	60%
2	50%	52%	88%	50%
3	--	--	18%	28%
4	60%	65.5%	25%	26%
5	50%, 65%	61%	52%, 88%	59%
6	--	--	38%	76%
7	45%	57.8%	65%	67.5%
8	--	--	60%	32%
9	--	--	53%	53%

Table 1: Pre-Stall and Fully developed Rotating Stall speeds.

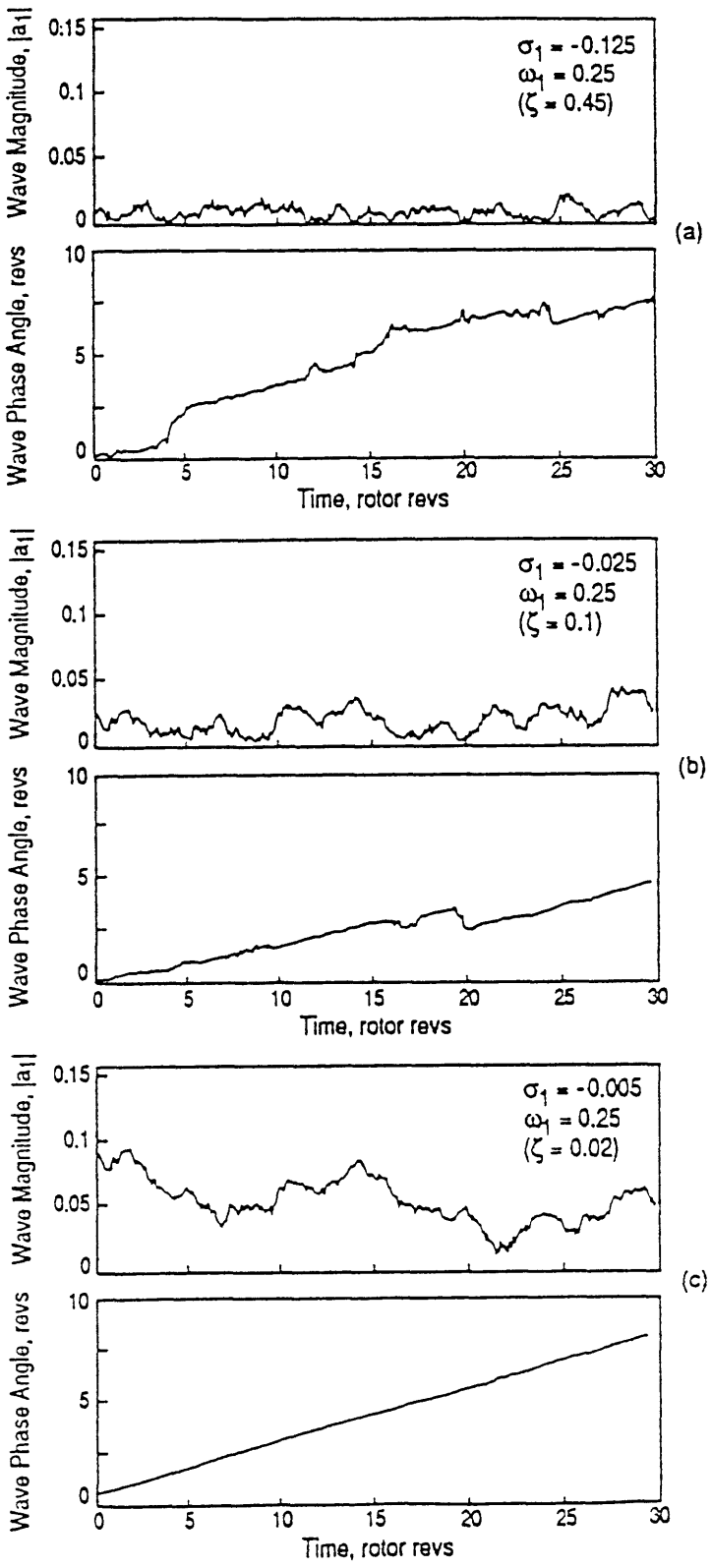

Figure 2.1: Simulated compressor 1st Fourier harmonic wave amplitude and phase, eq. (3).

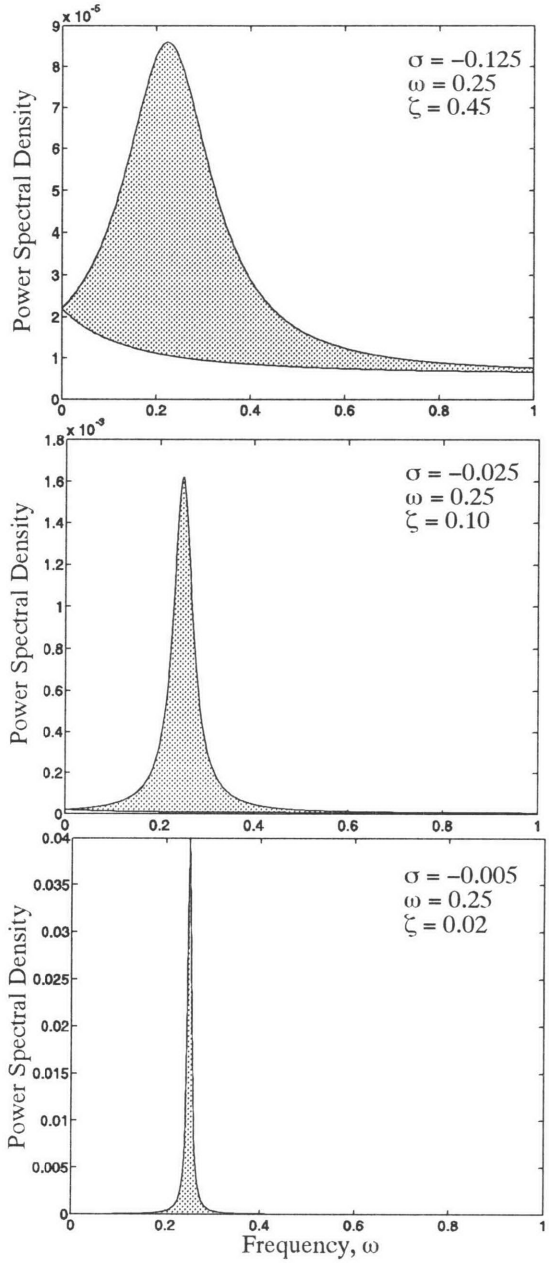

Figure 2.2: Spatial spectra of the simulations shown in Figure 2.1.

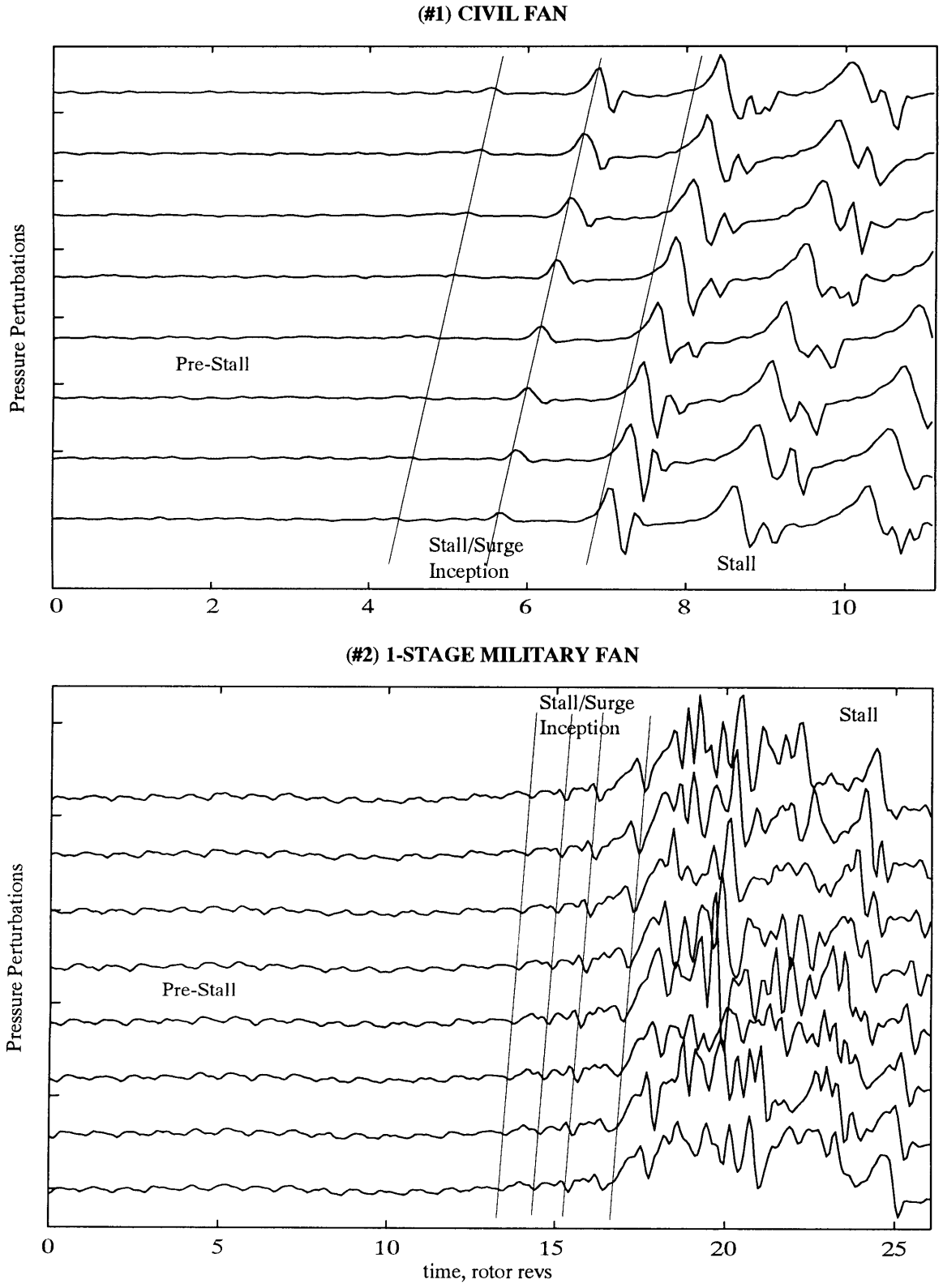

Figure 3.1: Time traces of the wall static pressure of all 9 compressors at 100% corrected speed. Data were collected using 8 sensors in all but one compressor (#8).

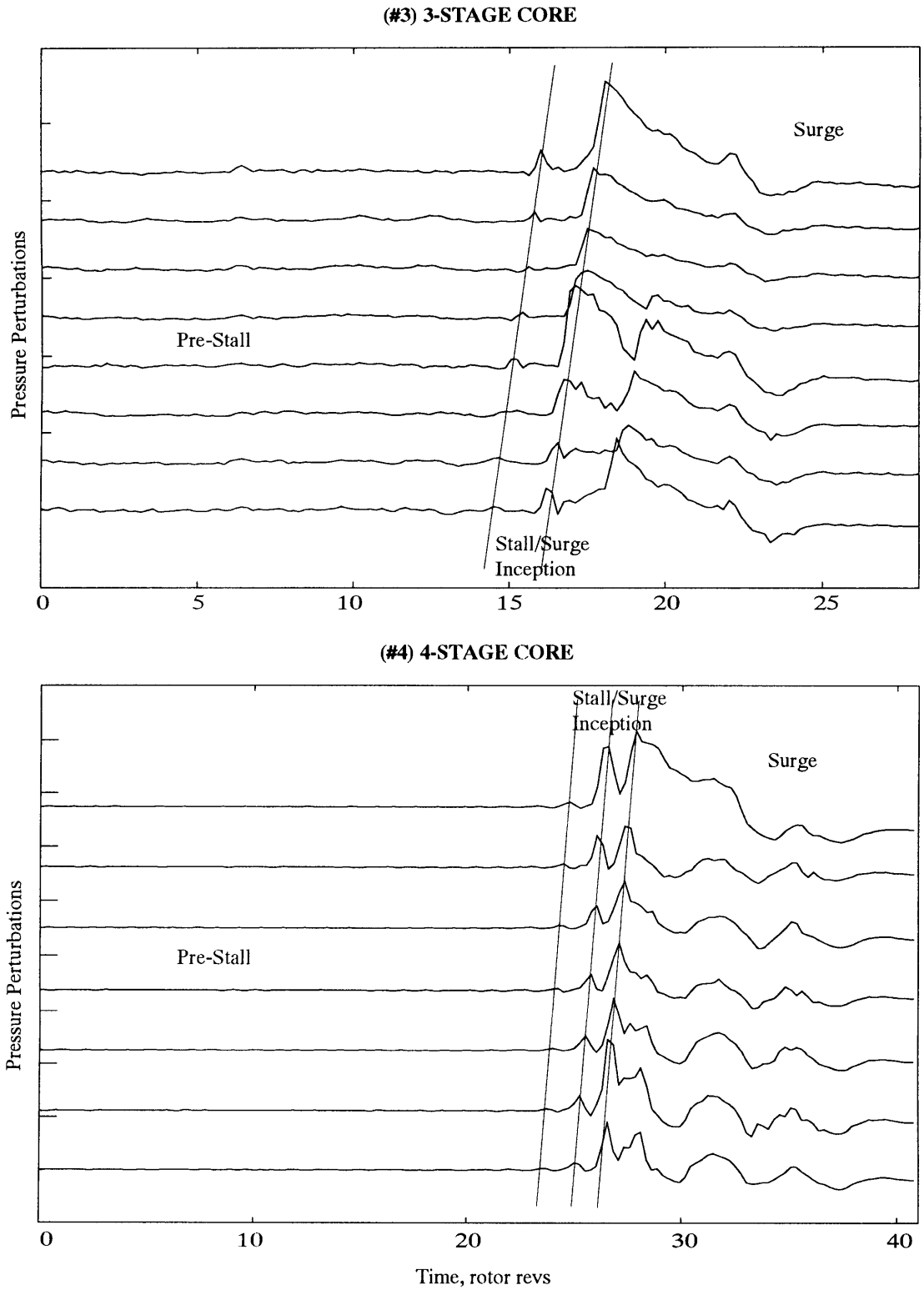

Figure 3.1: Continued.

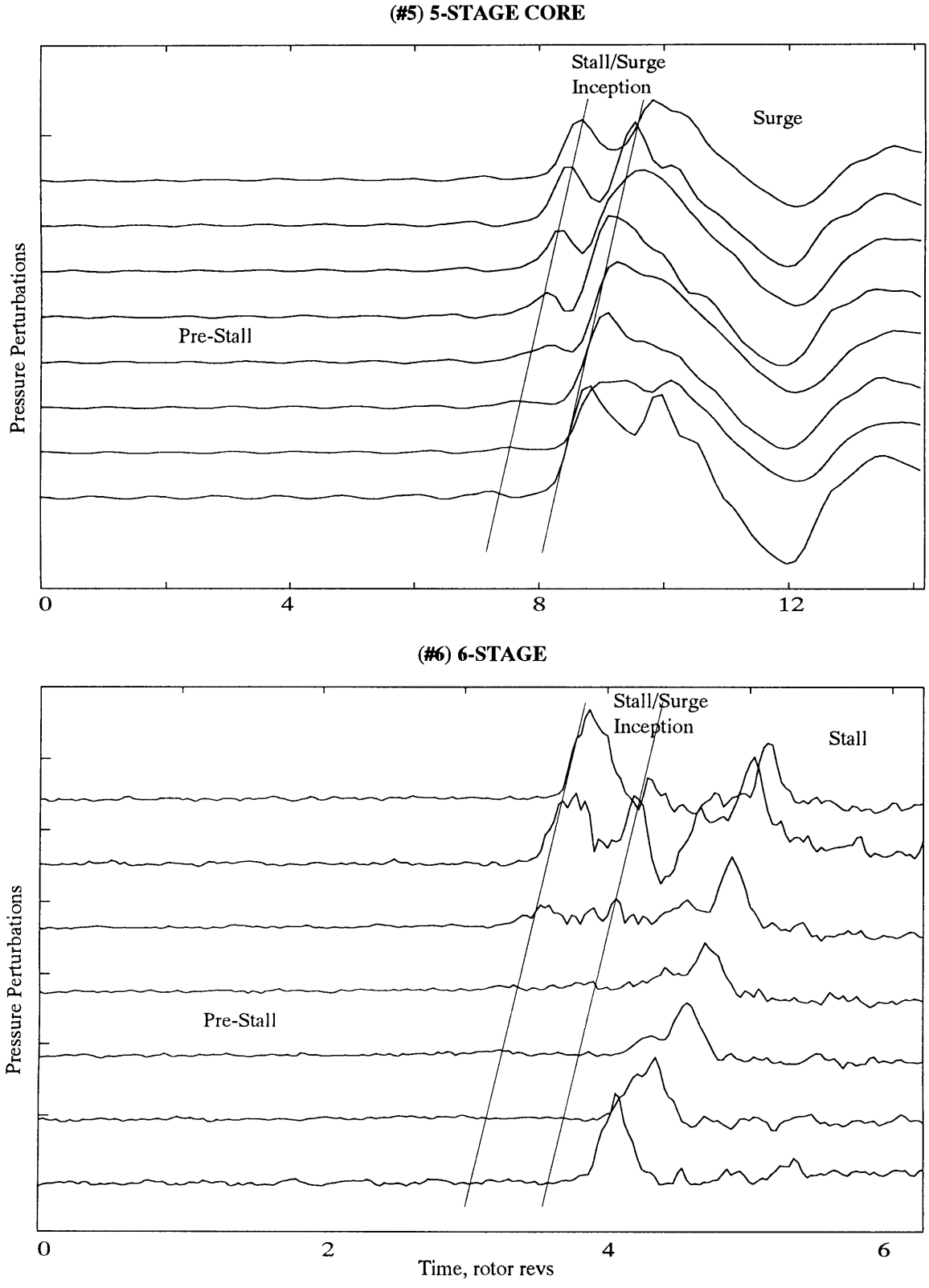

Figure 3.1: Continued.

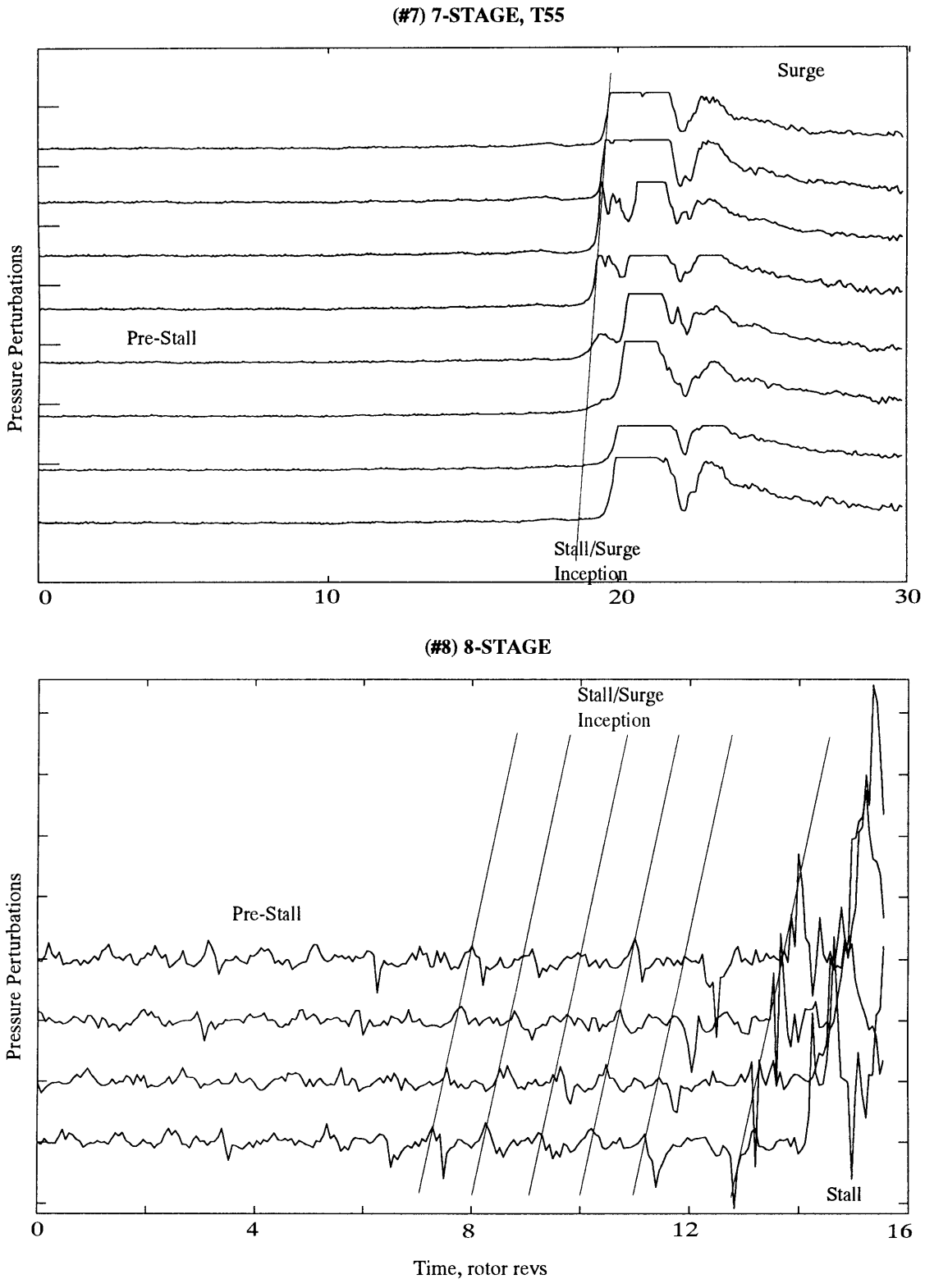

Figure 3.1: Continued.

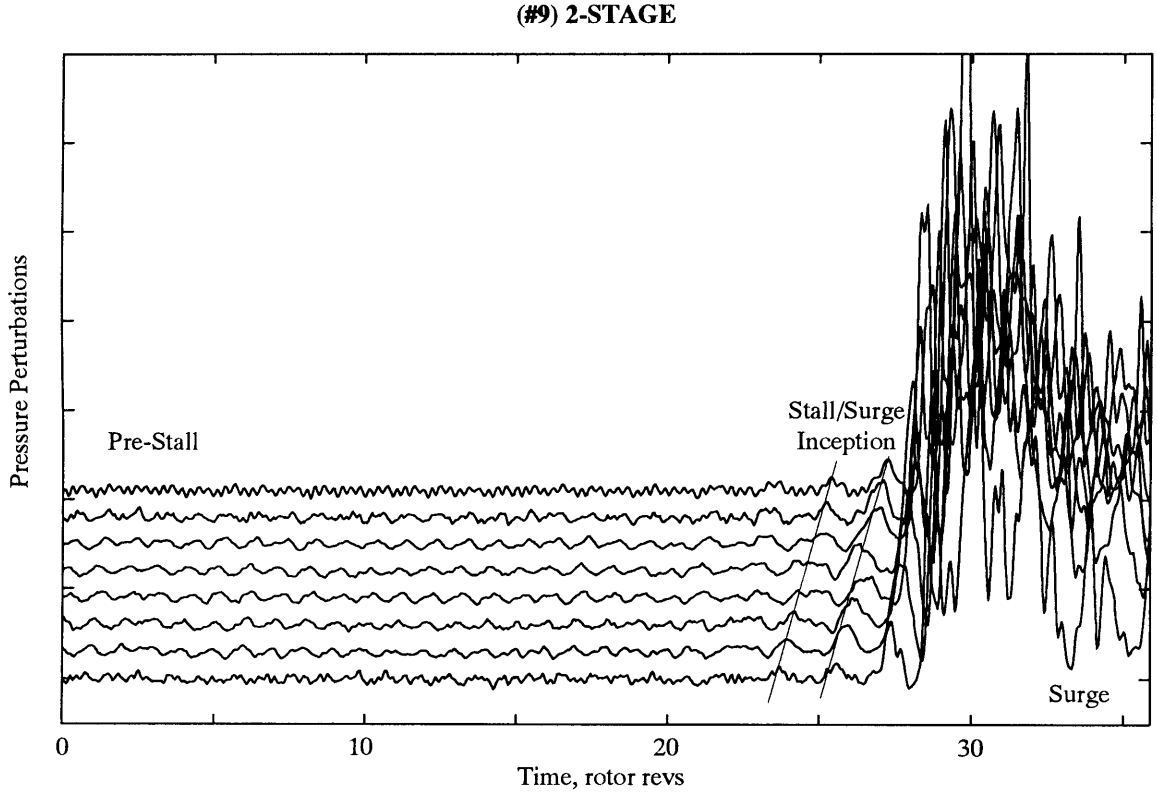

Figure 3.1: Continued.

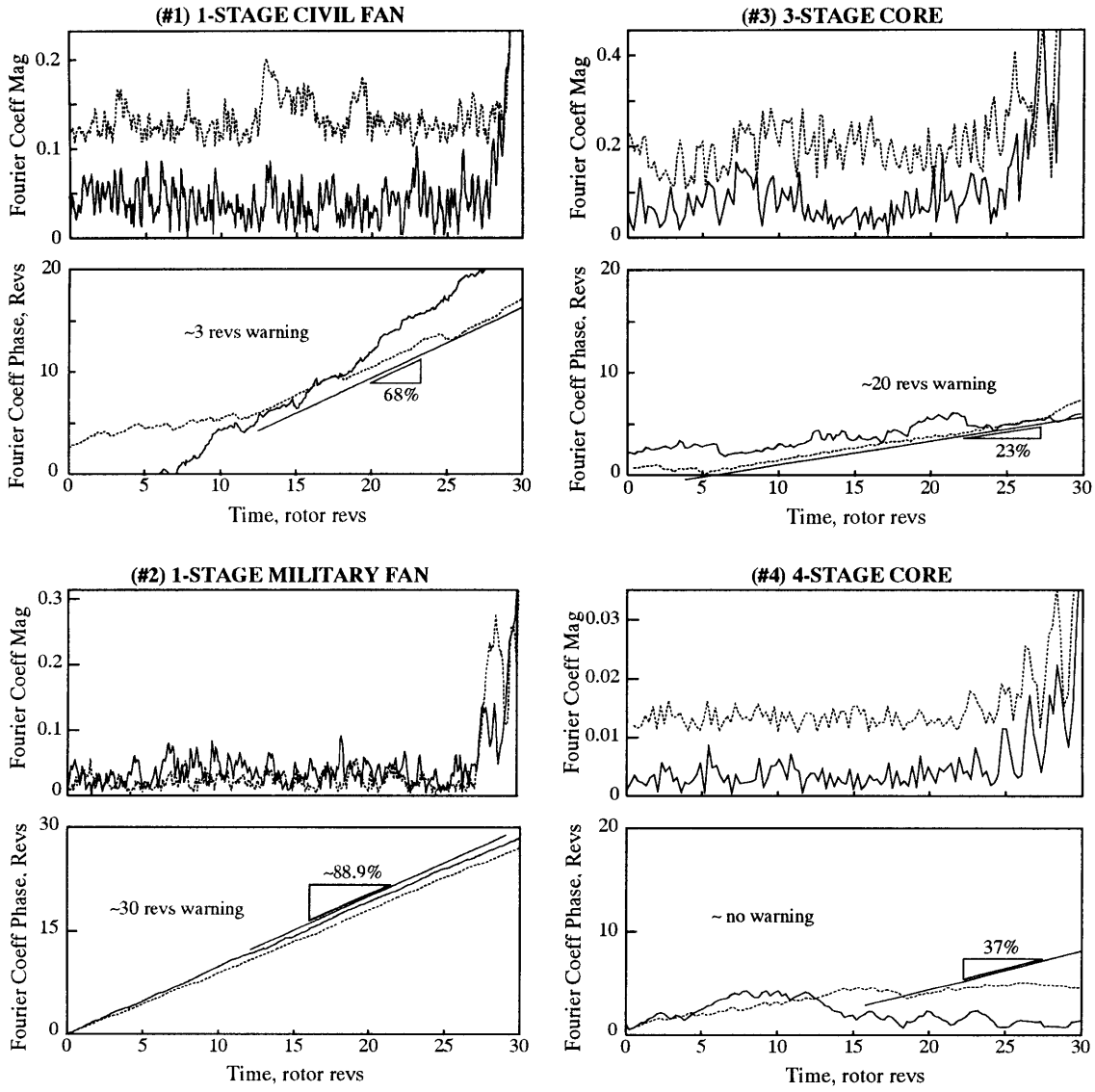

Figure 3.2: Magnitude and phase plots of the first (solid line) and second (dashed line), a_1 and a_2, spatial Fourier coefficients of the 100% runs. The slopes indicate the speed of the traveling as a percent of the rotor speed.

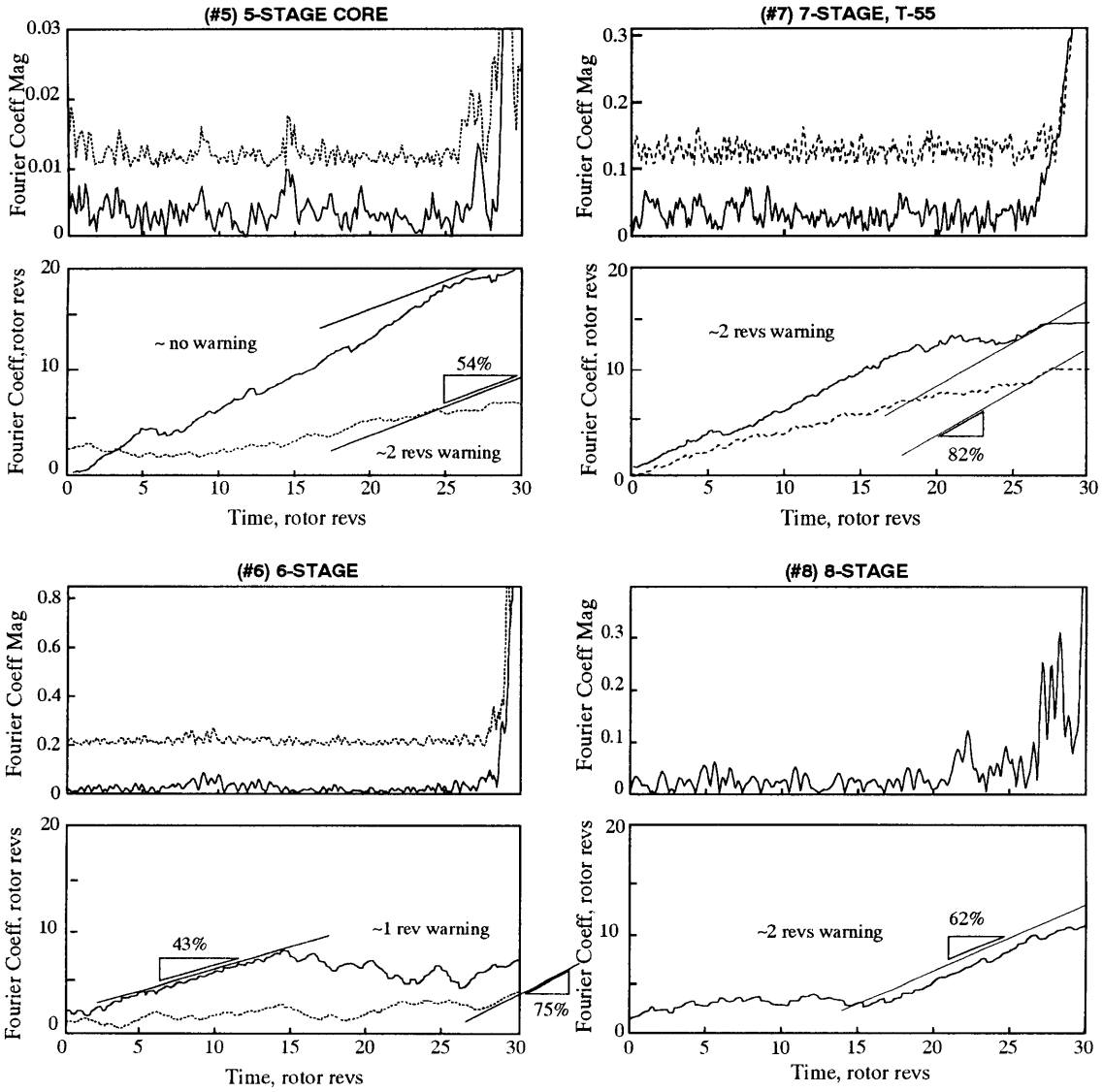

Figure 3.2: Continued.

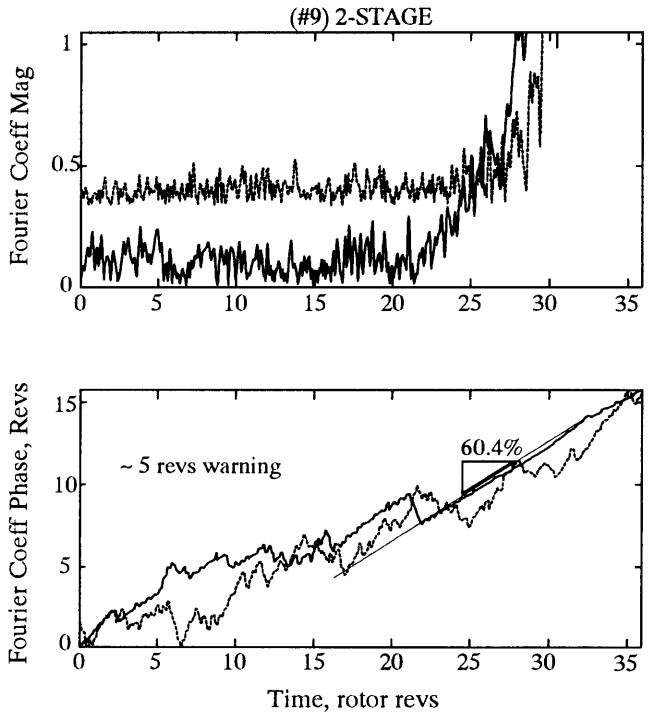

Figure 3.2: Continued.

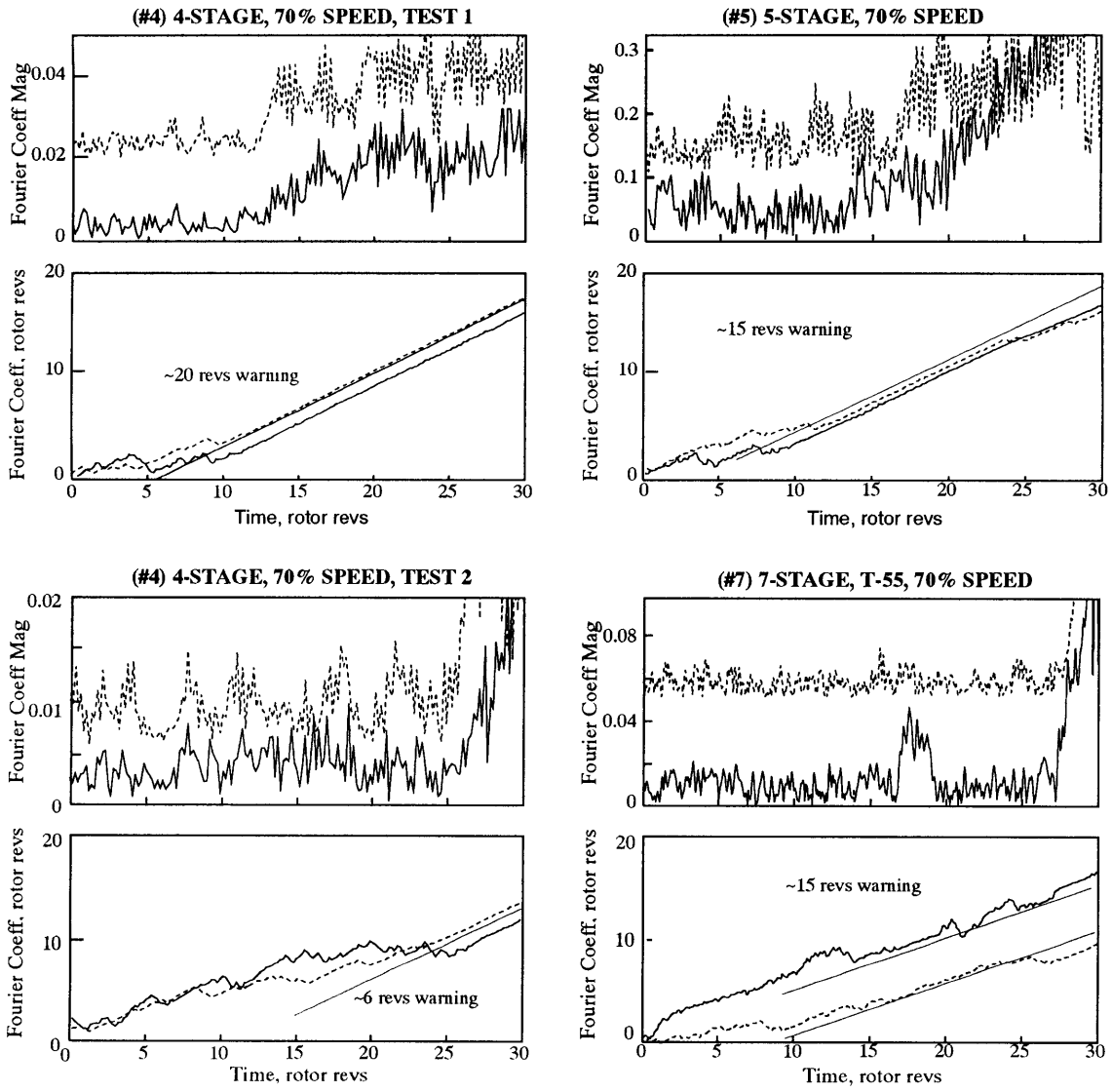

Figure 3.3: Magnitude and phase plots of the first (solid line) and second (dashed line), a_1 and a_2, spatial Fourier coefficients of the 70% runs. The slopes indicate the speed of the traveling as a percent of the rotor speed.

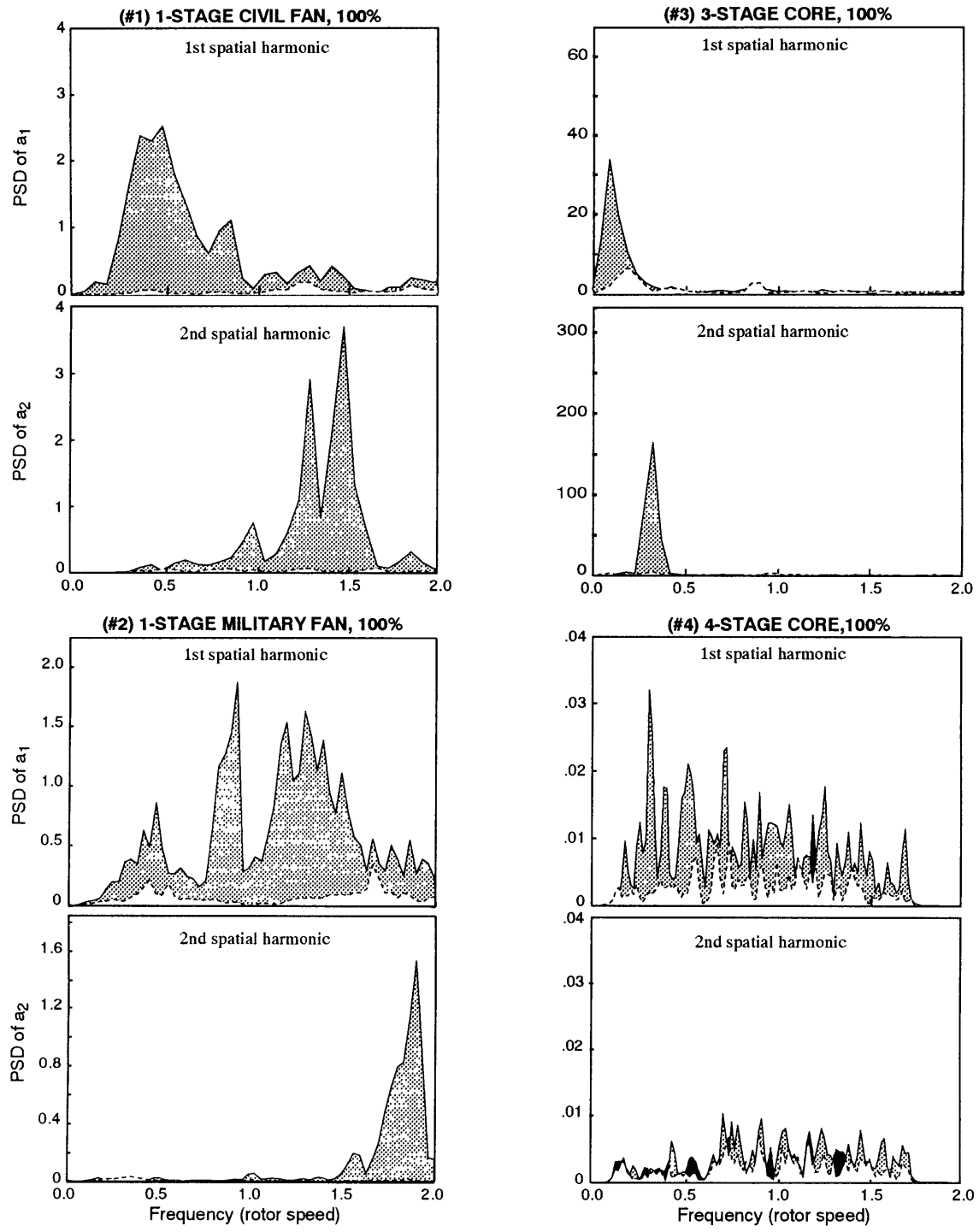

Figure 3.4: Power spectra of the first and the second spatial modes, a_1 and a_2, of all the100% runs. The forward traveling is shown by the solid line, while the negative traveling is shown by the dashed line.

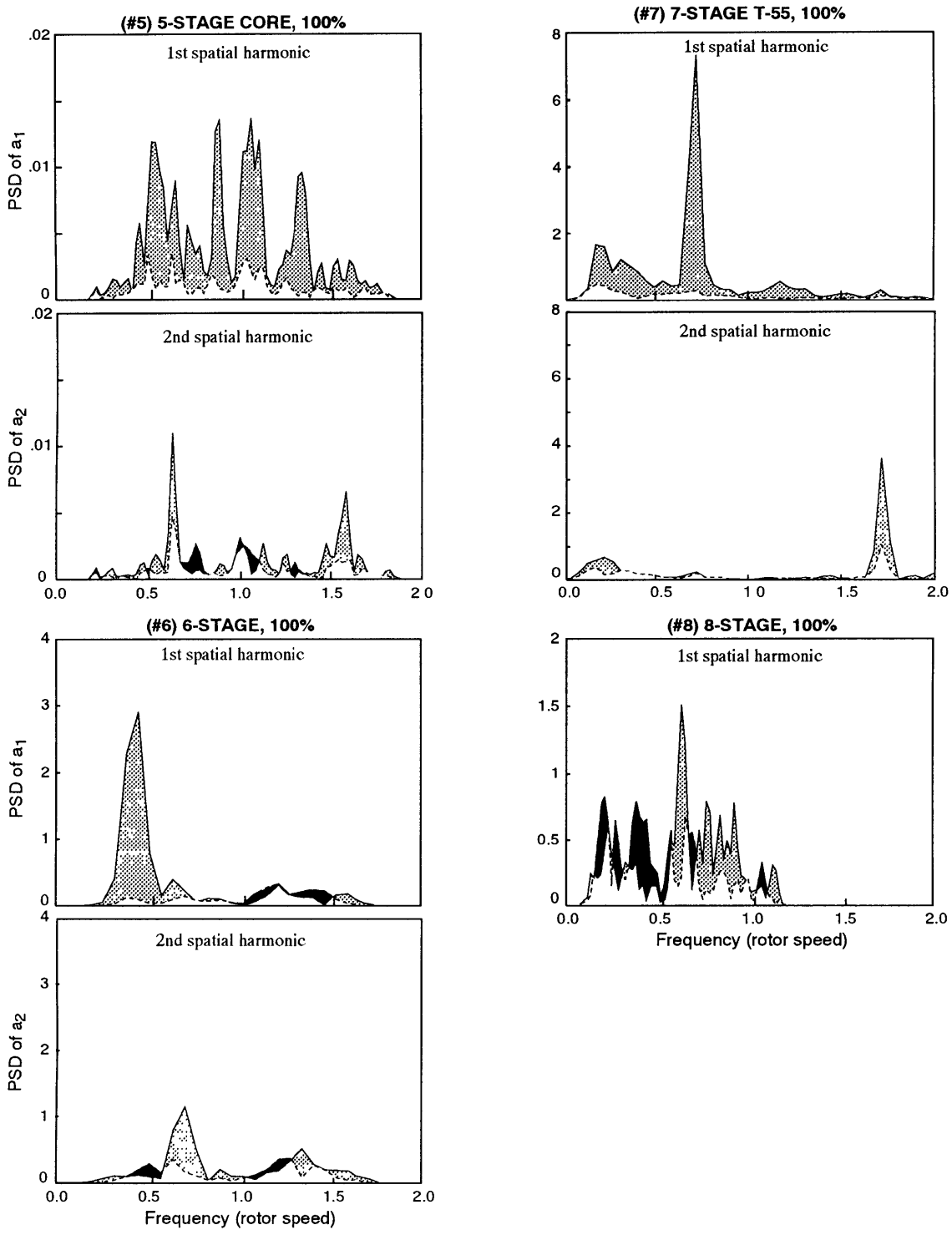

Figure 3.4: Continued.

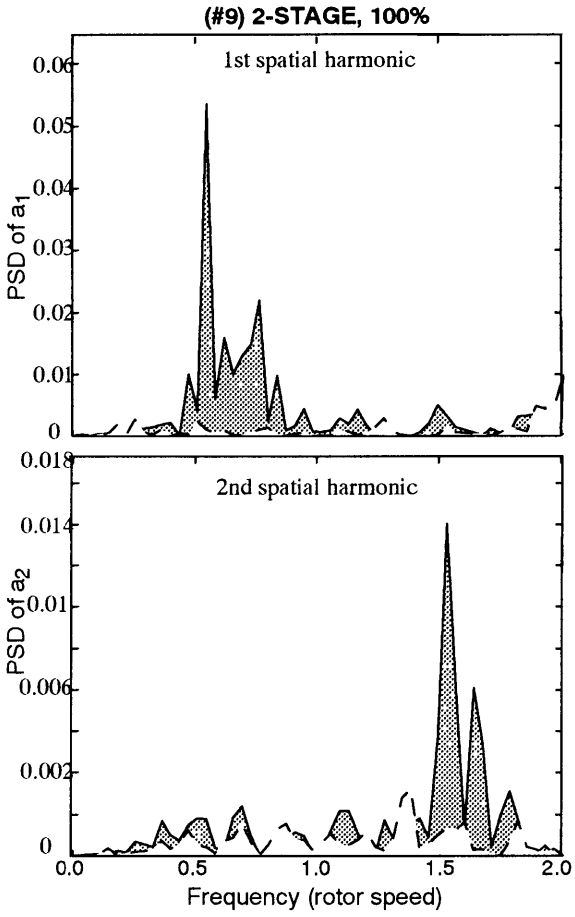

Figure 3.4: Continued.

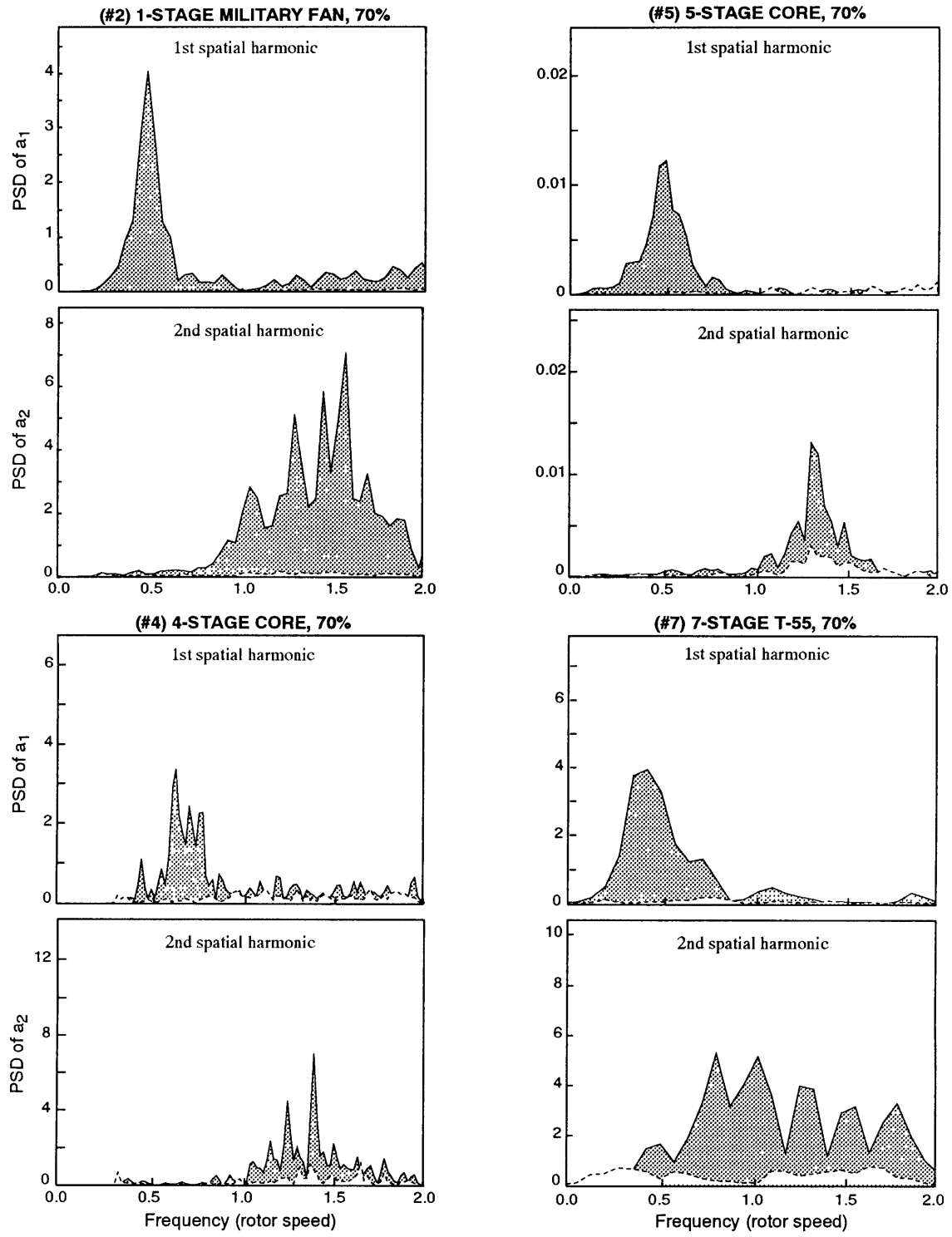

Figure 3.5: Power spectra of the first and the second spatial modes, a_1 and a_2, of all the 70% runs. The forward traveling is shown by the solid line, while the negative traveling is shown by the dashed line.

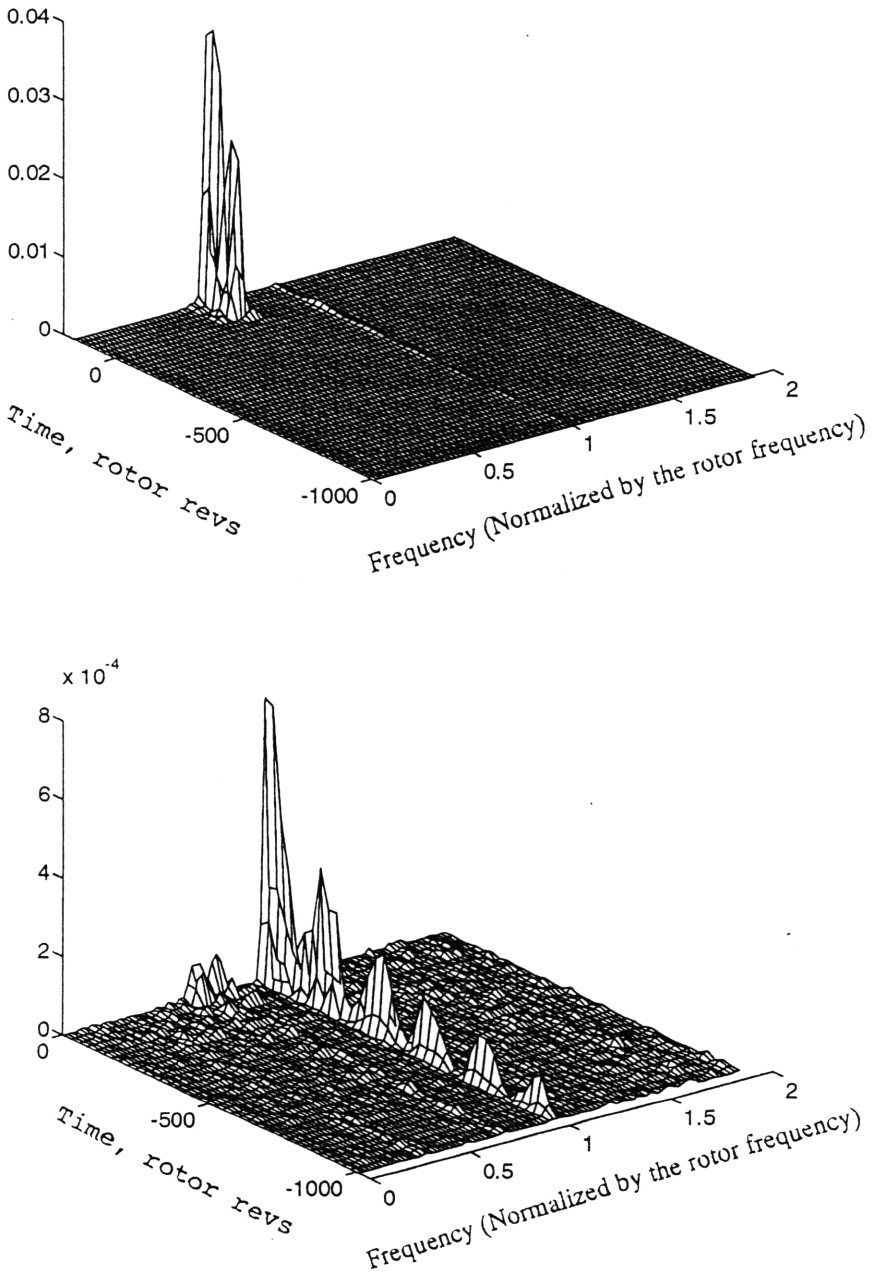

Figure 3.6: Time evolution of the PSD of the first spatial Fourier coefficient, a_1, for the 4-stage compressor at 70% corrected.

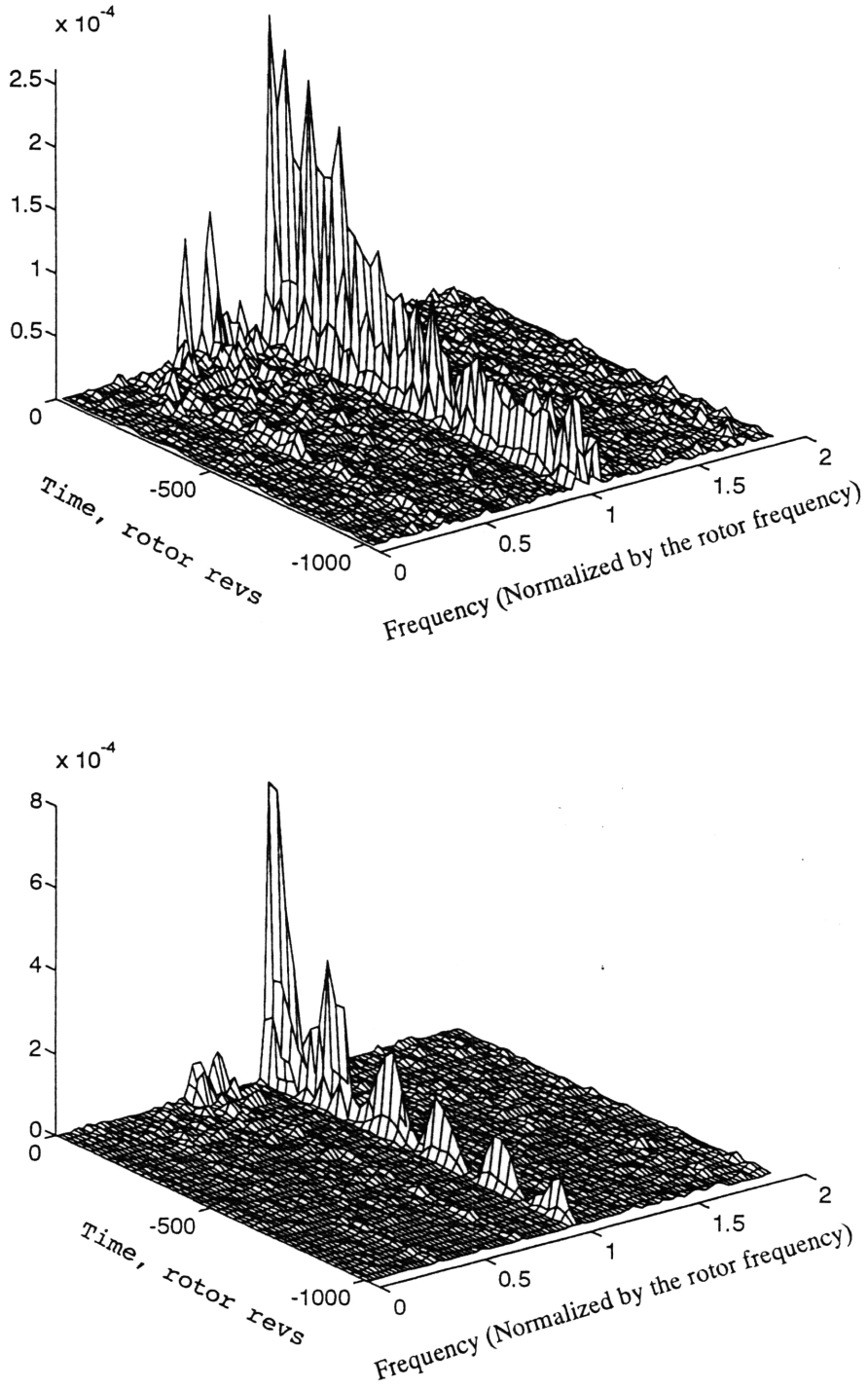

Figure 3.7: Influence of corrected speed on the time evolution of the first spatial mode of the 4-stage compressor.

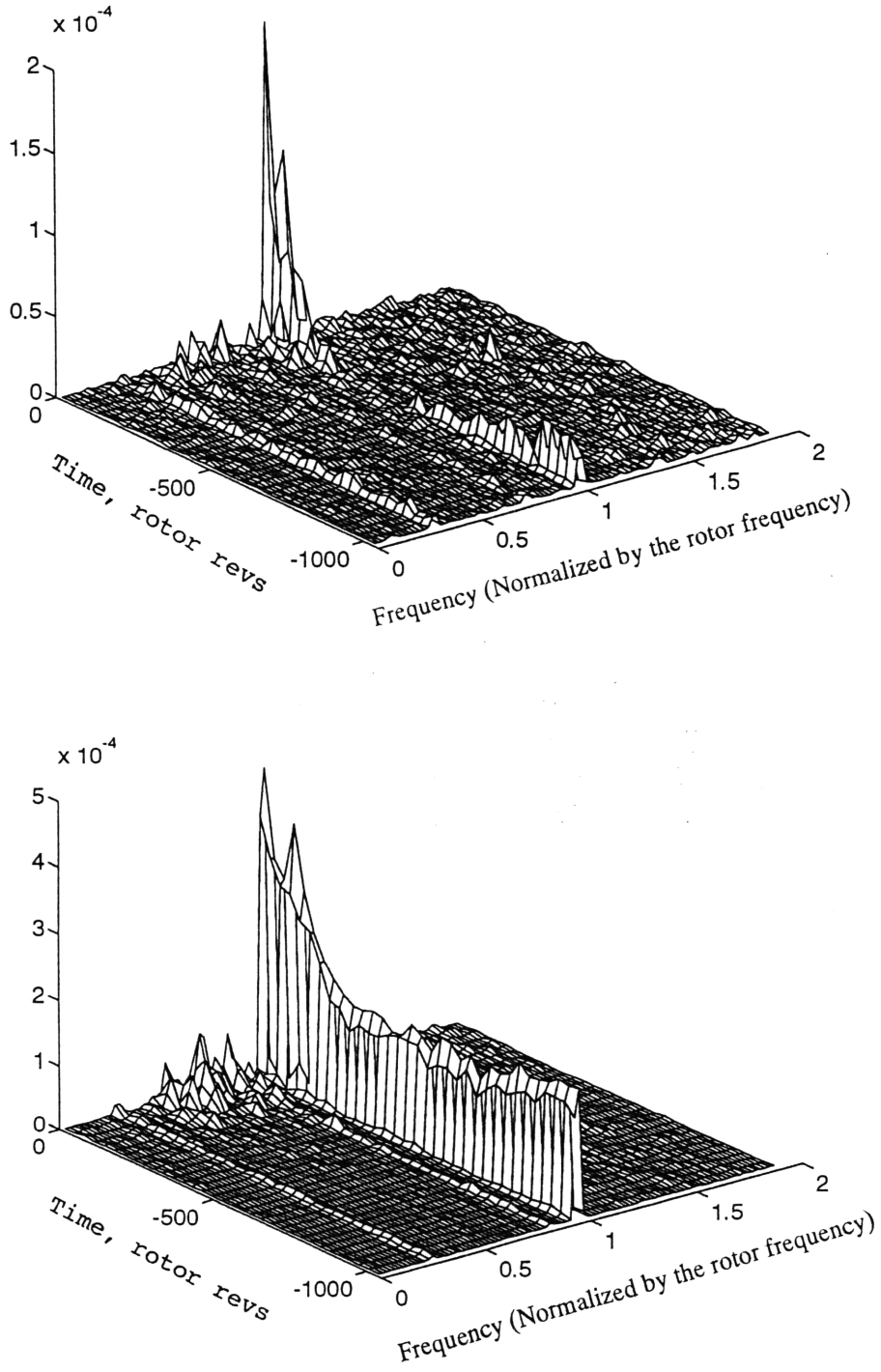

Figure 3.7: Continued.

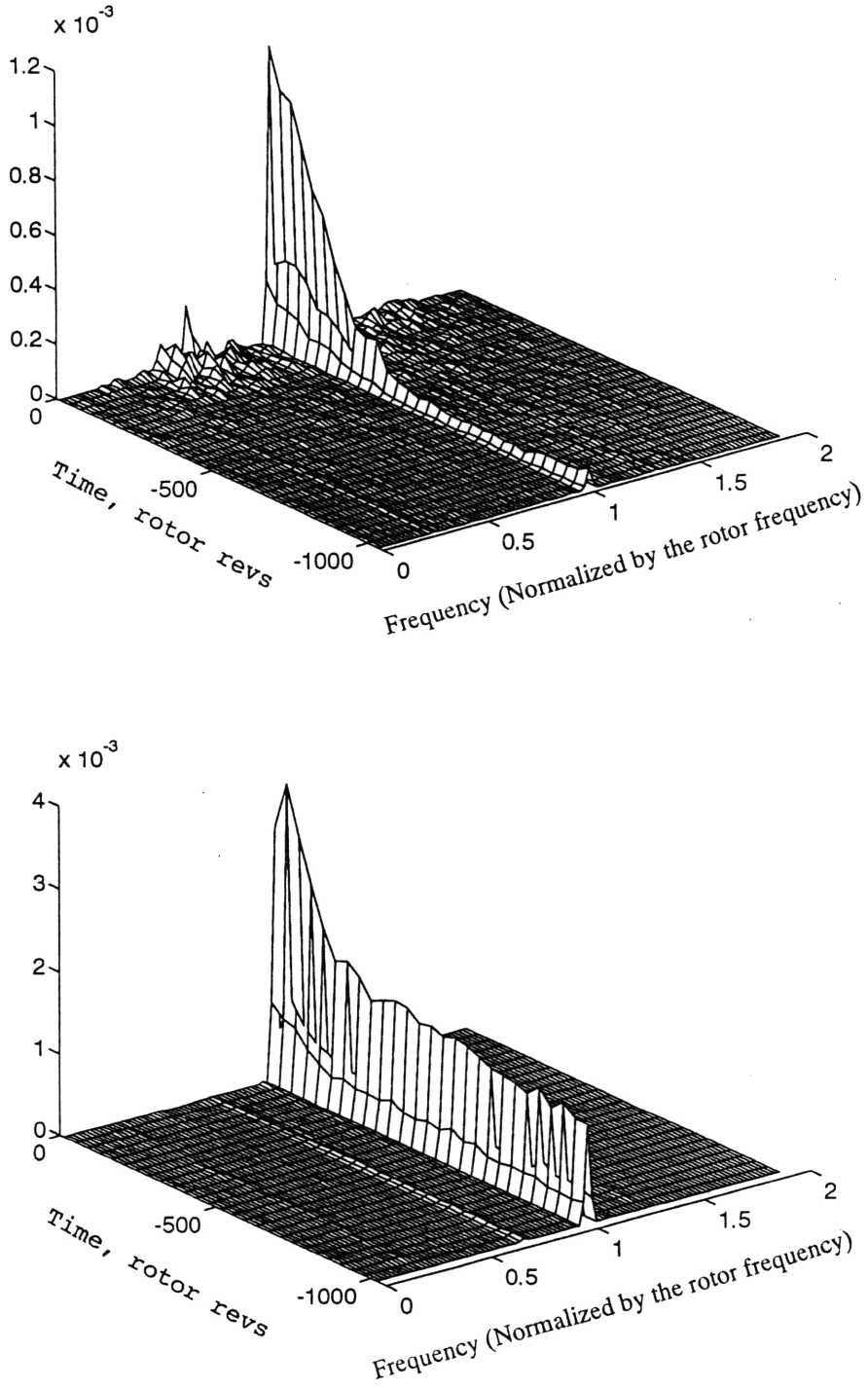

Figure 3.7: Continued.

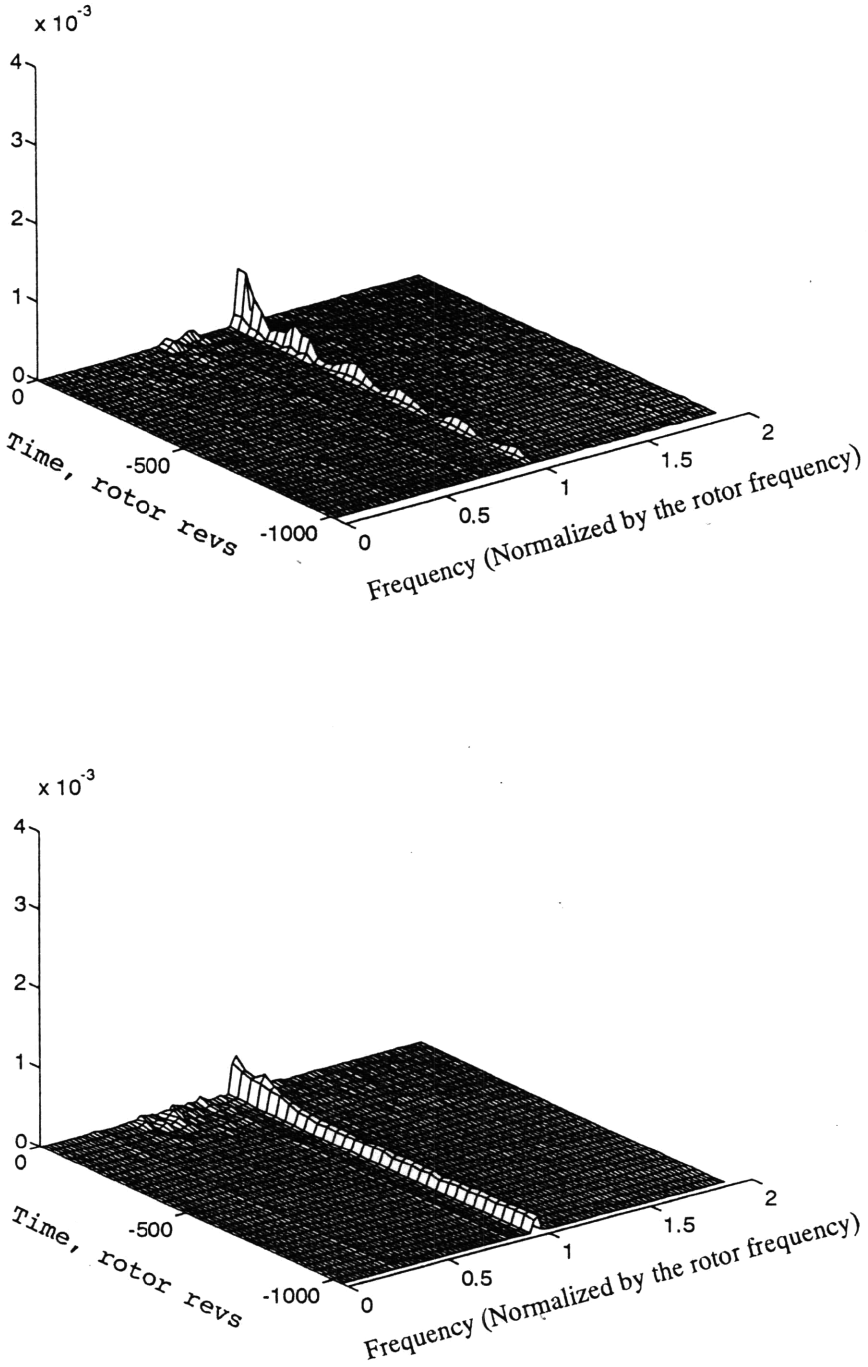

Figure 3.8: Influence of corrected speed on the time evolution of the forward first spatial mode of the 4-stage compressor. Same as Figure 3.7 but on the same scale.

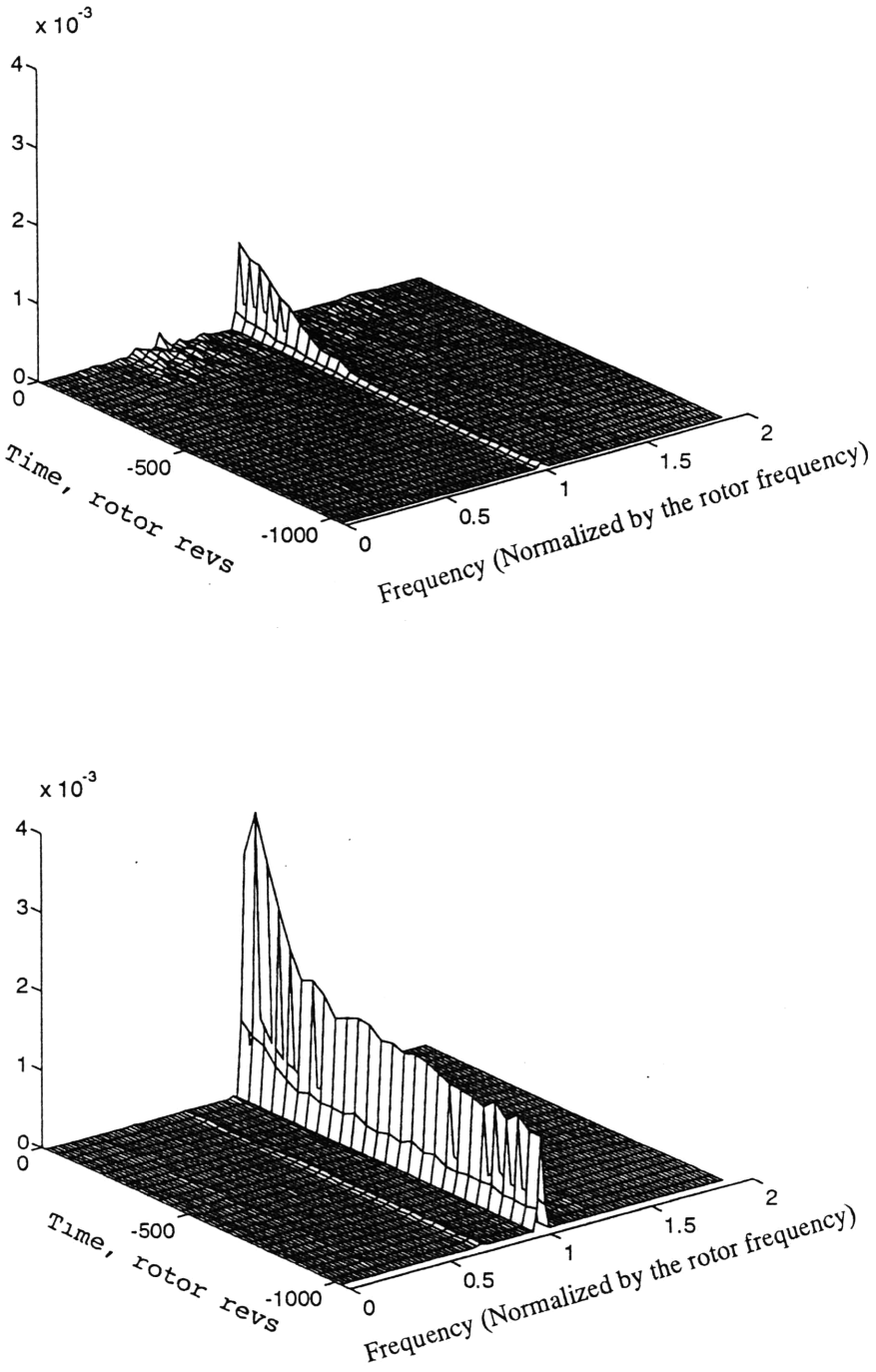

Figure 3.8: Continued.

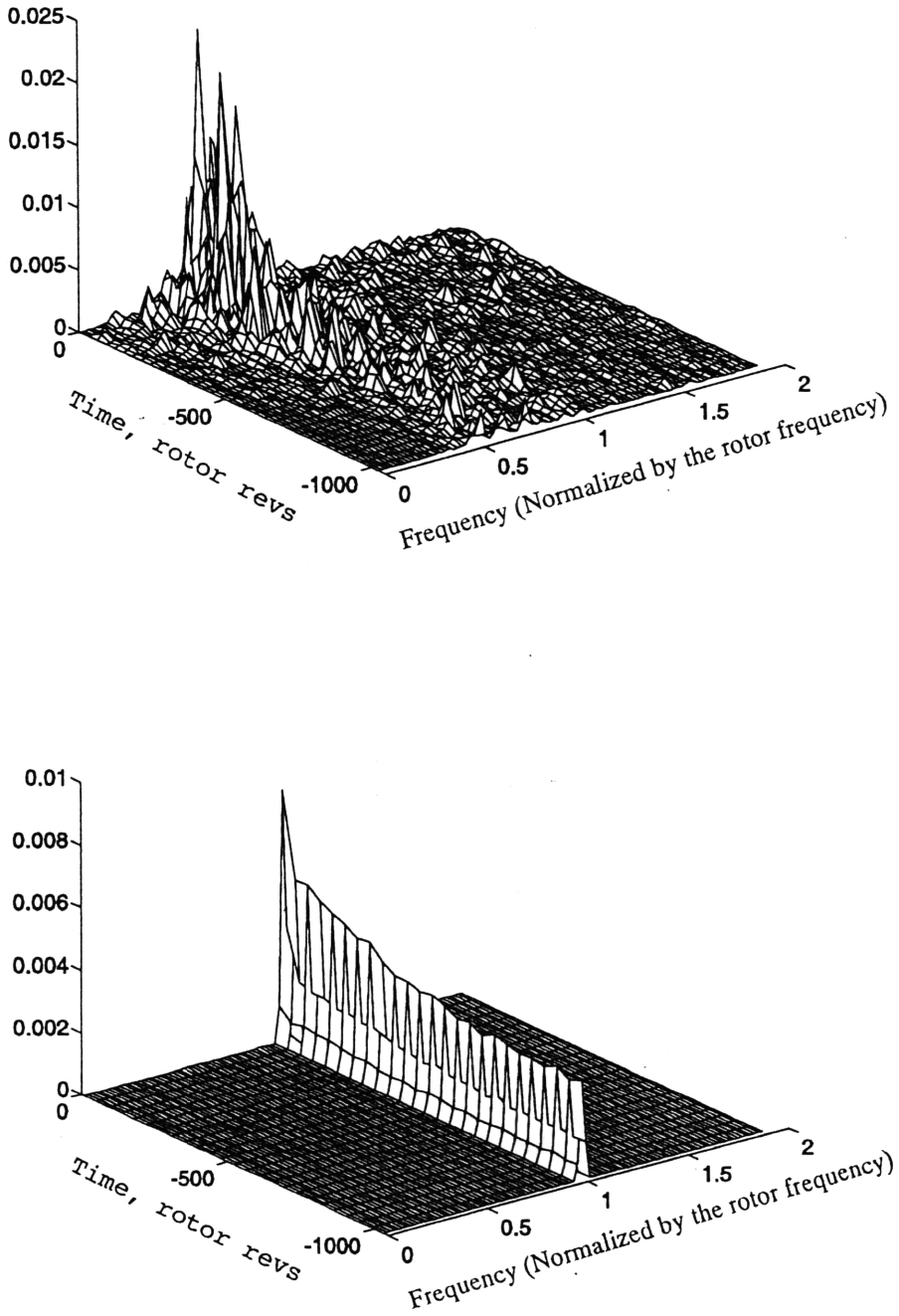

Figure 3.9: Waterfall of the first spatial Fourier coefficients, a_1, in the forward direction for compressors 2. The data is taken at 70% and 100% of the corrected speed.

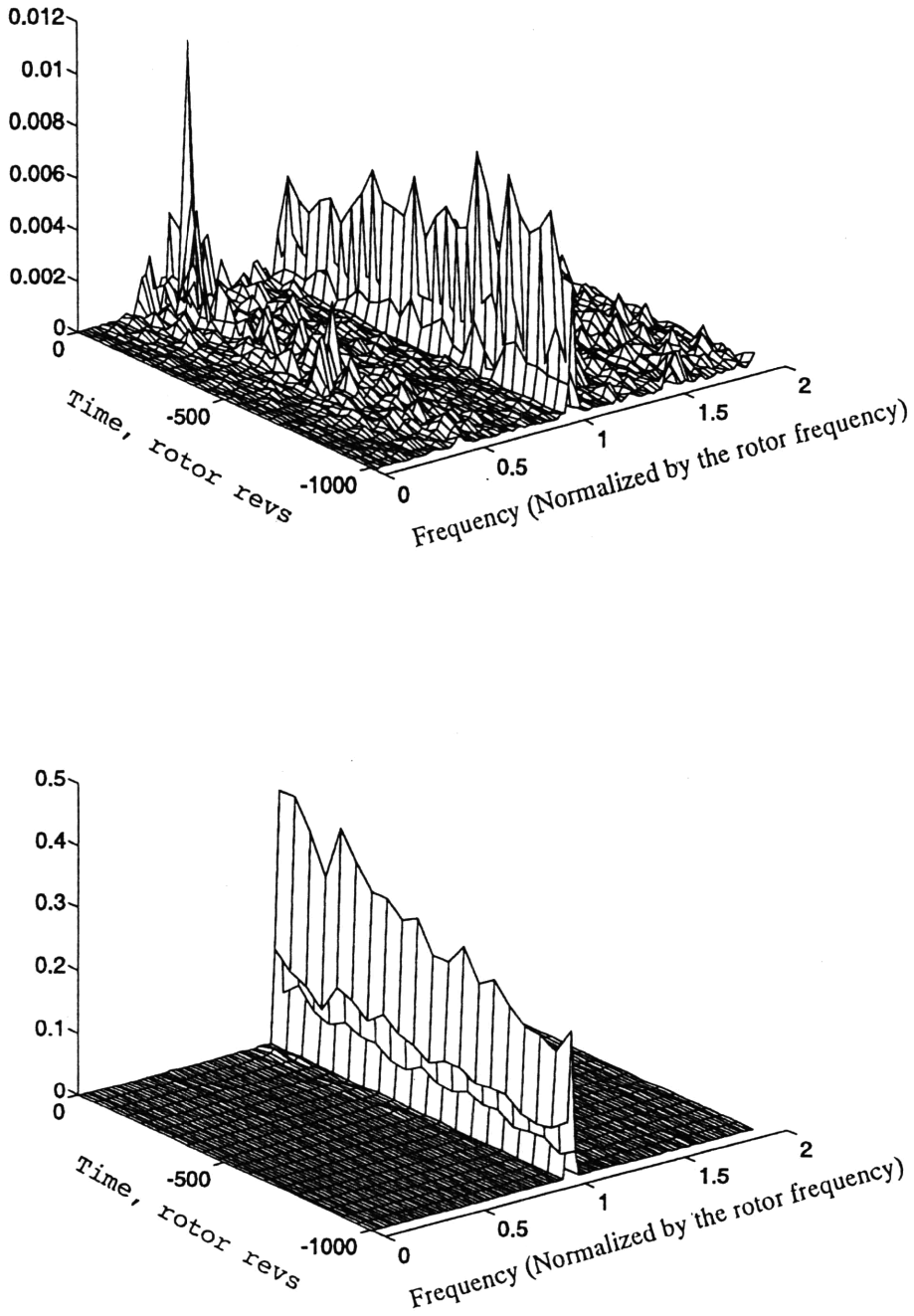

Figure 3.10: Waterfall of the first spatial Fourier coefficients, a_1, in the forward direction for compressors 5. The data is taken at 70% and 100% of the corrected speed.

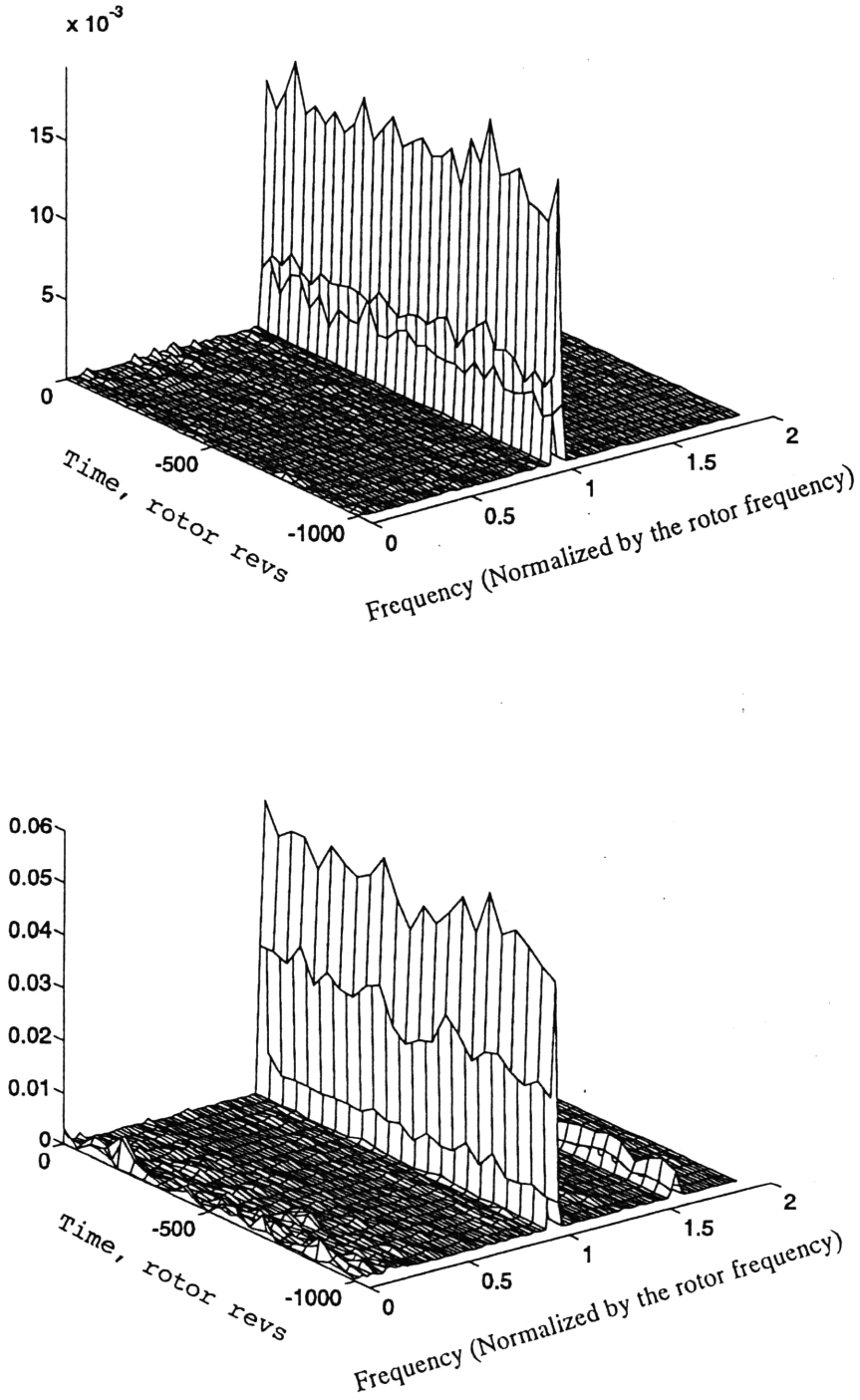

Figure 3.11: Waterfall of the first spatial Fourier coefficients, a_1, in the forward direction for compressors 7. The data is taken at 70% and 100% of the corrected speed (3.11a).

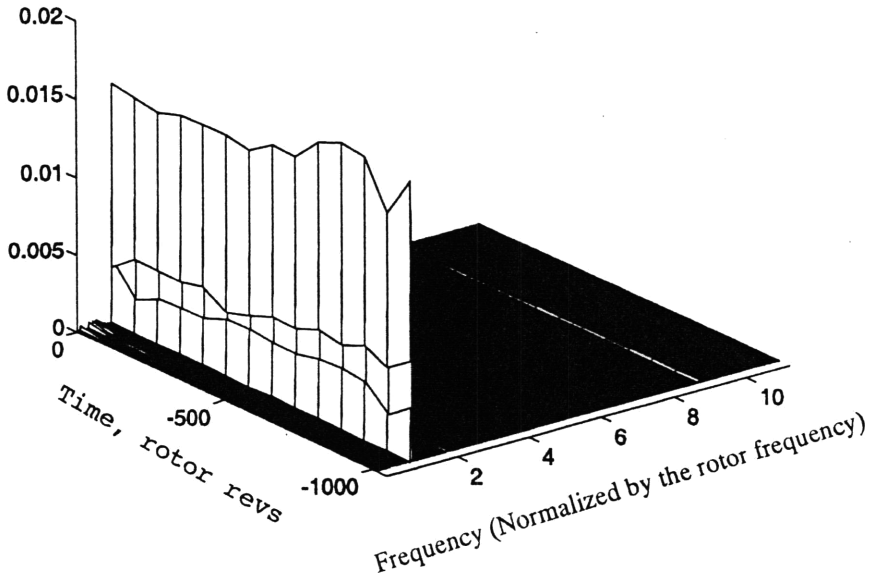

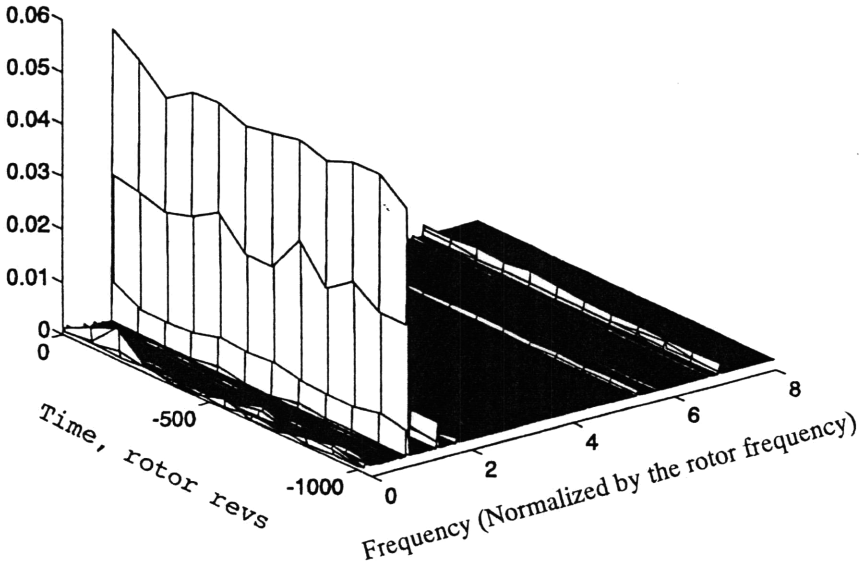

Figure 3.11: Continued (3.11b).

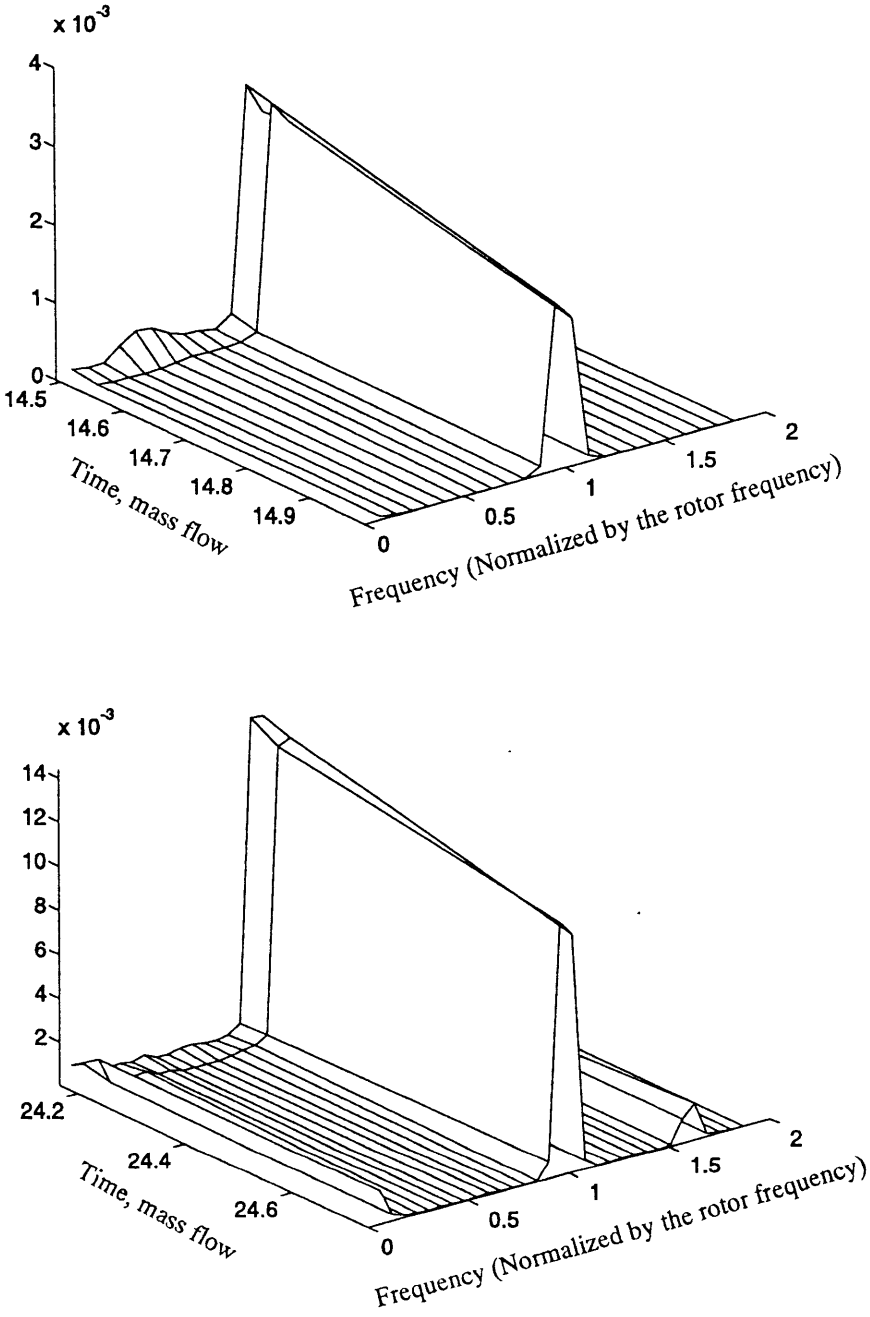

Figure 3.11: Continued (3.11c).

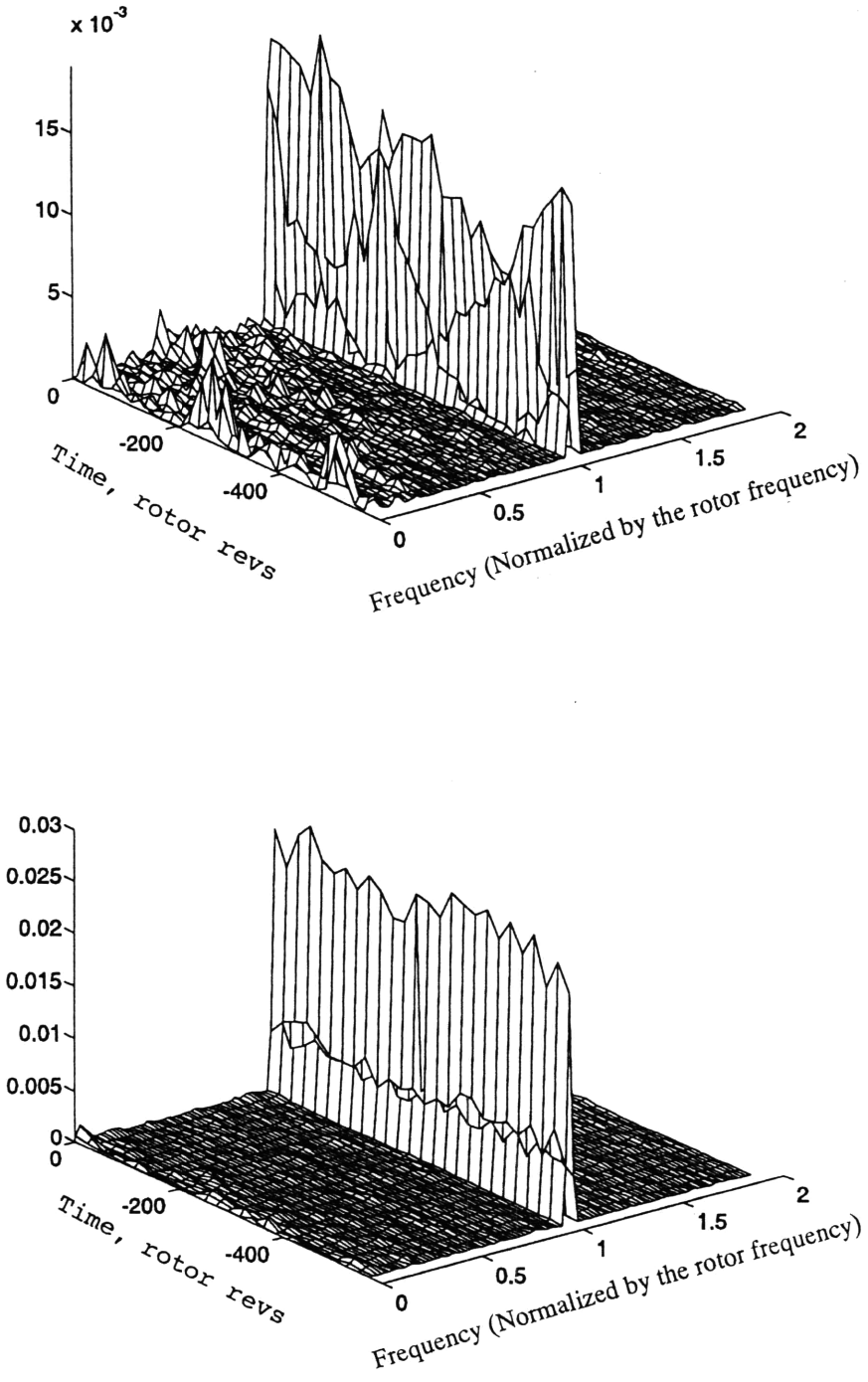

Figure 3.12: Waterfall of the first spatial Fourier coefficients, a_1, in the forward direction for compressors 8. The data is taken at 70% and 100% of the corrected speed (3.12a).

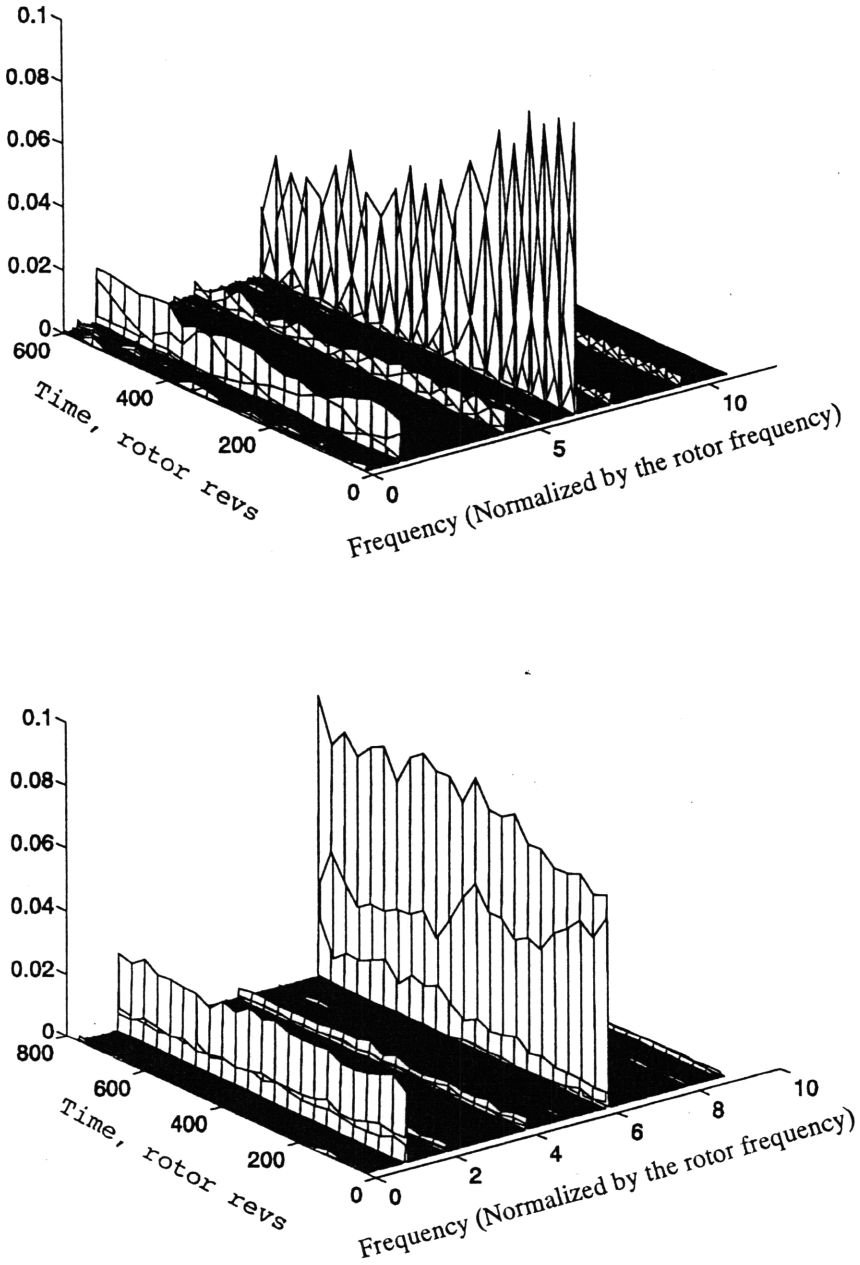

Figure 3.12: Continued (3.12b).

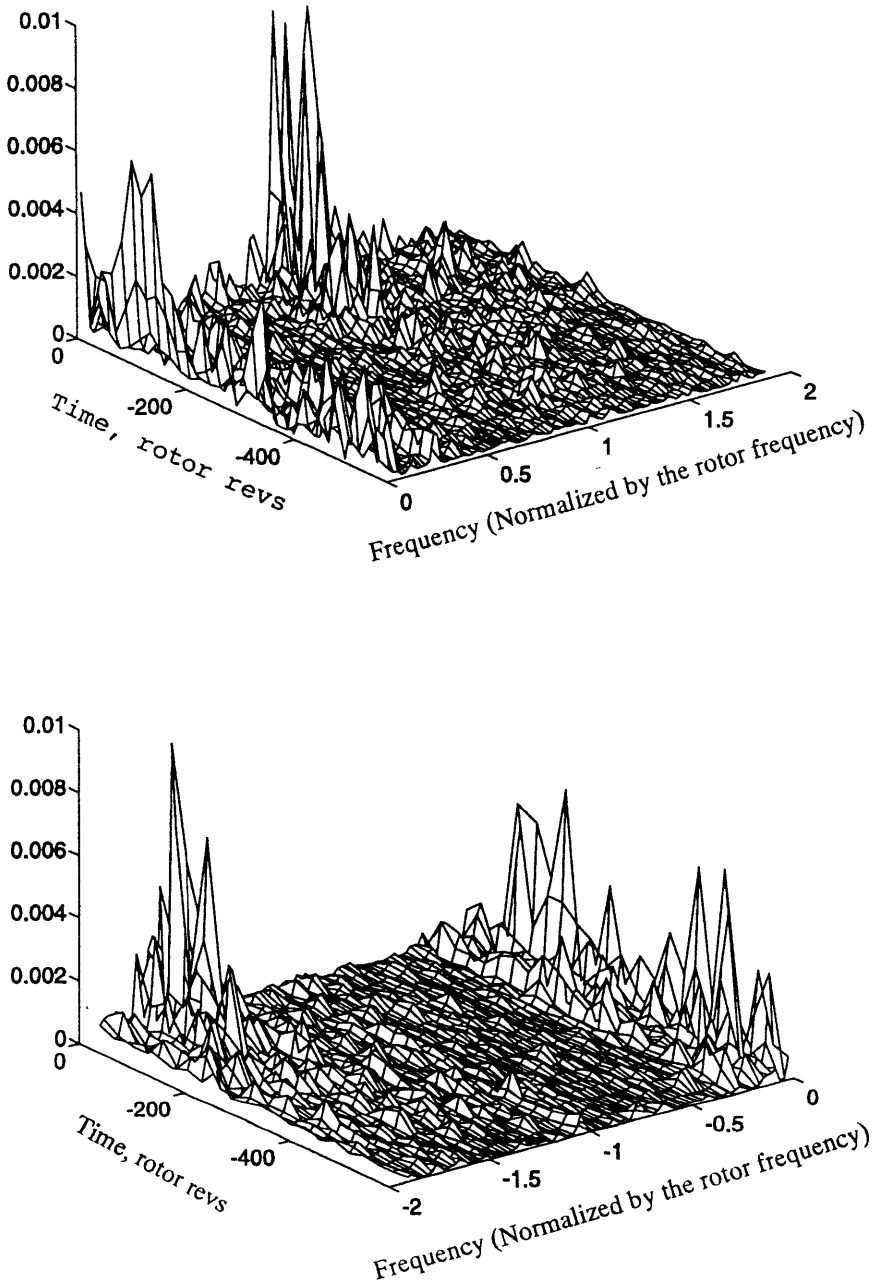

Figure 3.12: Continued (3.12c).

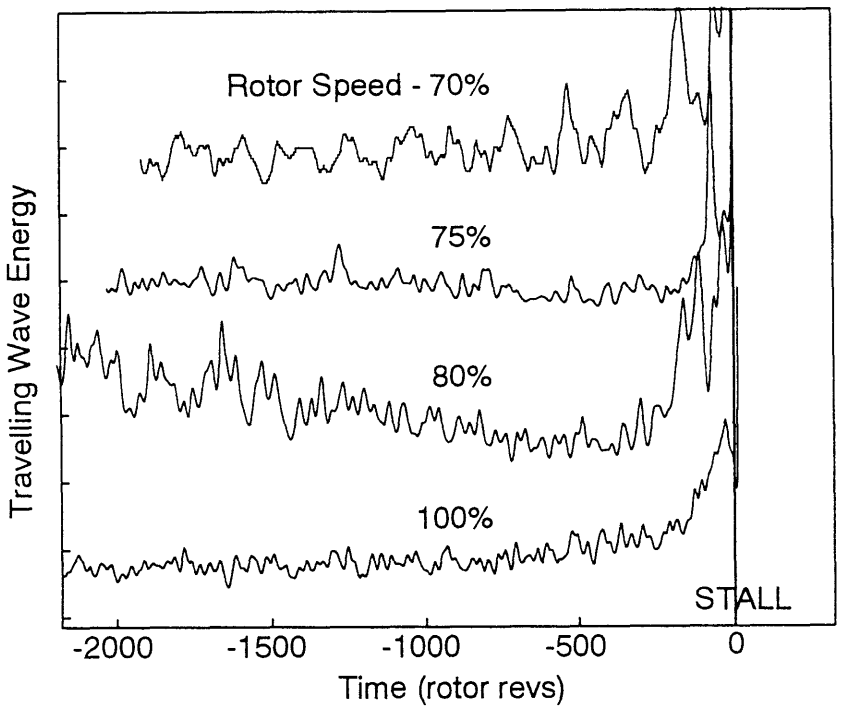

Figure 3.13: First spatial harmonic traveling wave energy during slow throttle traverse into stall for the 4-stage compressor.

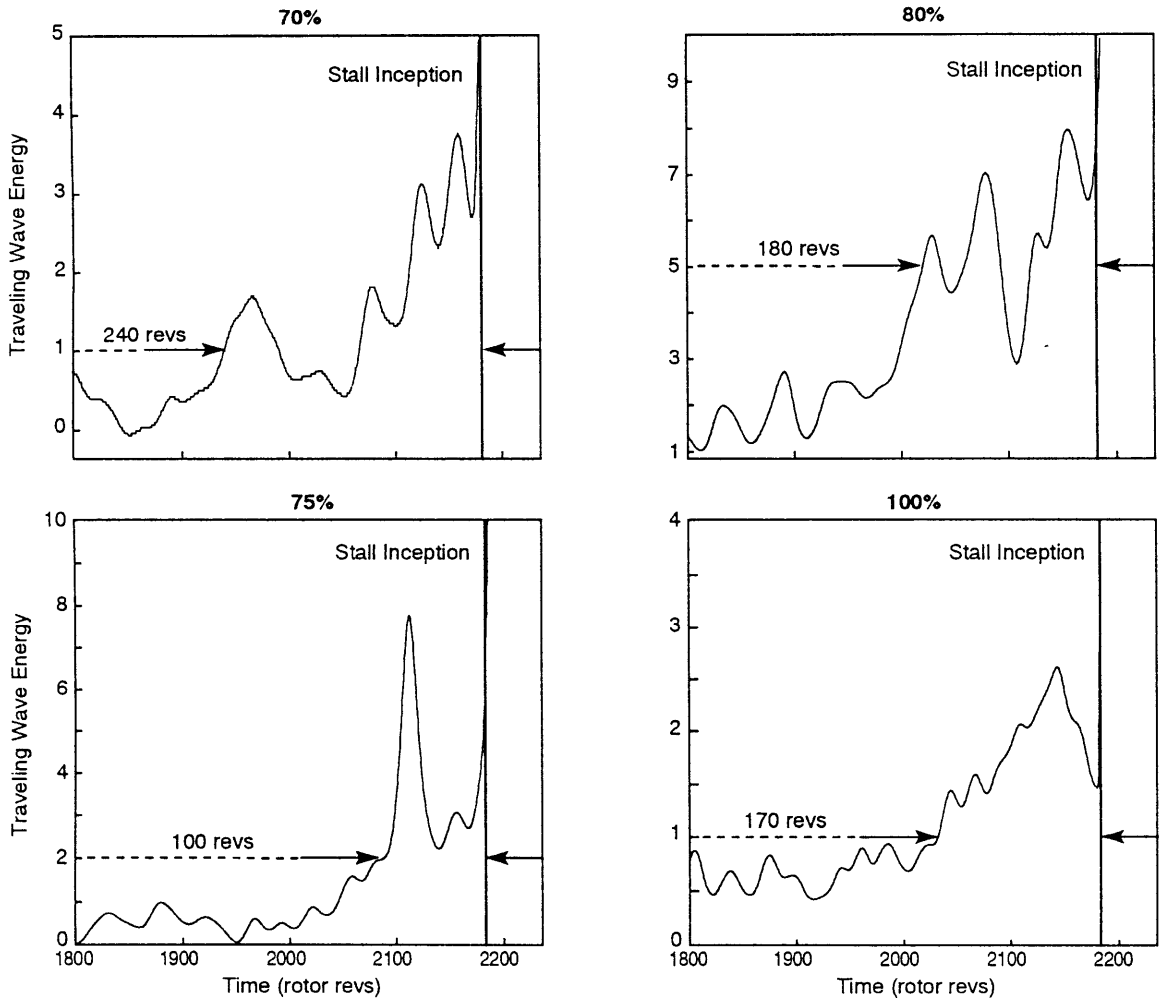

Figure 3.14: First spatial harmonic traveling wave energy during slow throttle traverse into stall for the 4-stage compressor in expanded scale.

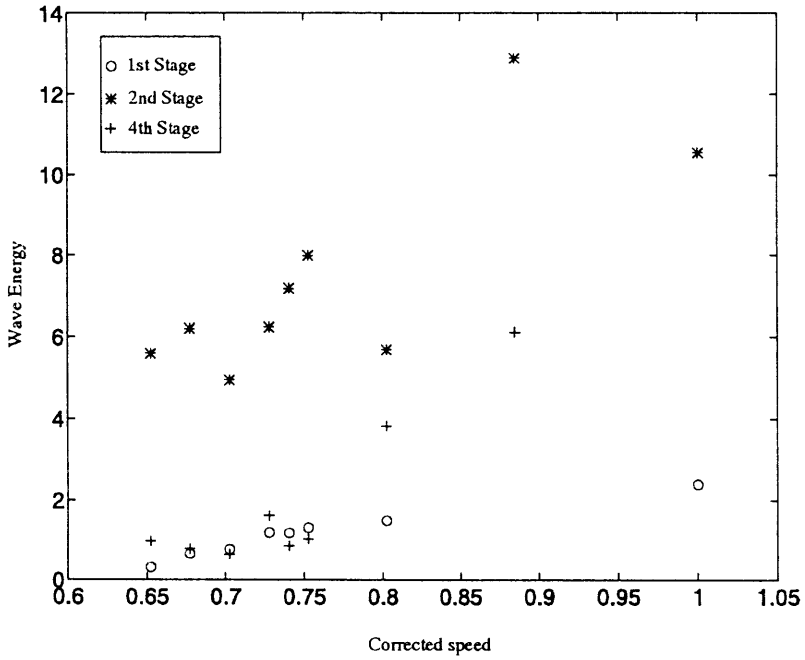

Figure 3.15: Traveling wave energy as a function of axial location and corrected speed.

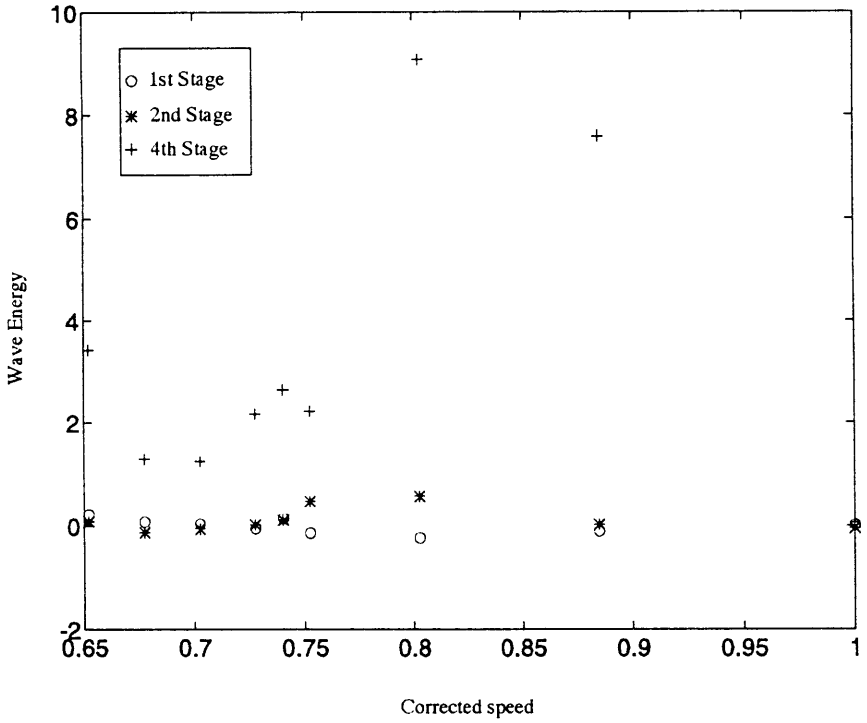

Figure 3.16: Traveling wave energy as a function of axial location and corrected speed.